AFRL-SN-RS-TR-1999-68
Final Technical Report
April 1999

SILICON INTERSUBBAND INFRARED LASERS

Lionel R. Friedman

APPROVED FOR PUBLIC RELEASE; DISTRIBUTION UNLIMITED.

**AIR FORCE RESEARCH LABORATORY
SENSORS DIRECTORATE
ROME RESEARCH SITE
ROME, NEW YORK**

19990524 059

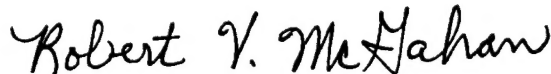AFRL-SN-RS-TR-1999-68 has been reviewed and is approved for publication.

APPROVED: *Richard A. Soref*

RICHARD A. SOREF
Project Engineer

FOR THE DIRECTOR: *Robert V. McGahan*

ROBERT V. McGAHAN, Technical Advisor
Electromagnetics Technology Division
Sensors Directorate

REPORT DOCUMENTATION PAGE			*Form Approved* OMB No. 0704-0188

Public reporting burden for this collection of information is estimated to average 1 hour per response, including the time for reviewing instructions, searching existing data sources, gathering and maintaining the data needed, and completing and reviewing the collection of information. Send comments regarding this burden estimate or any other aspect of this collection of information, including suggestions for reducing this burden, to Washington Headquarters Services, Directorate for Information Operations and Reports, 1215 Jefferson Davis Highway, Suite 1204, Arlington, VA 22202-4302, and to the Office of Management and Budget, Paperwork Reduction Project (0704-0188), Washington, DC 20503.

1. AGENCY USE ONLY *(Leave blank)*	2. REPORT DATE April 1999	3. REPORT TYPE AND DATES COVERED Final Mar 97 - Sep 98

4. TITLE AND SUBTITLE SILICON INTERSUBBAND INFRARED LASERS	5. FUNDING NUMBERS C - F30602-97-C-0081 PE - 61102F PR - 2305 TA - D2 WU - P4
6. AUTHOR(S) Lionel R. Friedman	

7. PERFORMING ORGANIZATION NAME(S) AND ADDRESS(ES) Lionel R. Friedman 49 Winfield Road Holden MA 01520	8. PERFORMING ORGANIZATION REPORT NUMBER N/A

9. SPONSORING/MONITORING AGENCY NAME(S) AND ADDRESS(ES) Air Force Research Laboratory/SNHC 80 Scott Drive Hanscom AFB MA 01731-2909	10. SPONSORING/MONITORING AGENCY REPORT NUMBER AFRL-SN-RS-TR-1999-68

11. SUPPLEMENTARY NOTES

Air Force Research Laboratory Project Engineer: Richard A. Soref/SNHC/(781) 377-2380

12a. DISTRIBUTION AVAILABILITY STATEMENT Approved for public release; distribution unlimited.	12b. DISTRIBUTION CODE

13. ABSTRACT *(Maximum 200 words)*

In this document, we report on design of silicon-based intersubband lasers. There are: (1) The symmetric strain symmetrized Si/Ge intersubband laser, (2) The asymmetric design to obtain higher gain, (3) Studies and calculations of in-plane energy dispersion of Si/Ge superlattices needed for above designs. The p-i-p diode laser of (2) is grown up a relaxed Si (0.25) buffer layer on Si, with Ge quantum wells and Si barriers in a 3:1 thickness ratio.

14. SUBJECT TERMS Intersubband Lasers, Quantum Wells, Superlattices, Carrier Lifetimes, Silicon, Germanium			15. NUMBER OF PAGES 48
			16. PRICE CODE

17. SECURITY CLASSIFICATION OF REPORT UNCLASSIFIED	18. SECURITY CLASSIFICATION OF THIS PAGE UNCLASSIFIED	19. SECURITY CLASSIFICATION OF ABSTRACT UNCLASSIFIED	20. LIMITATION OF ABSTRACT UL

Table of Contents

0.1 Introduction: Novel Designs for Silicon-Based Unipolar Intersubband Lasers

This contract has focused on designs of silicon-based quantum well intersubband lasers. There are several strong motivations for this effort. First, present infrared lasers are fabricated from III-V semiconductors and so require hybrid integration with silicon based microelectronics. To have a fully silicon based laser monolithically integrable with advanced silicon microelectronics would be a significant advance with respect to cost and simplicity of processing. Silicon and silicon/germanium have not been used for optical applications primarily because of the fact that their energy band gaps are indirect. This means that in order for an electron to absorb radiation (a photon) and be promoted from the valence to the conduction band, crystal momentum must be supplied by the lattice vibrations (phonons). Similarly, in order for an electron and hole to recombine and emit radiation, crystal momentum must be provided by the phonons, substantially reducing the efficiency and making the process strongly temperature dependent. This limitation (the indirect bandgap) can be avoided by considering transitions within the conduction band or valence band alone, but not between them, i.e. (unipolar) intersubband processes but not (bipolar) interband processes. We have studied such intersubband transition in confined quantum well structures where the energy levels and hence the photon energy are tunable by changing the dimensions of the quantum well and barrier. This is another major advantage of quantum well bandgap engineering. We have considered only unipolar hole injection in the valence band because the conduction band offsets are negligibly small for growth on a pure silicon substrate. A finite conduction band offset is possible for growth on a silicon/germanium alloy buffer layer, but this was not considered in the present work for operation in the conduction band. The silicon/germanium alloy buffer layer was considered, however, for the strain-symmetrized silicon/germanium short period superlattice for operation in the valence band, described later in this report.

1.1 Comparison with Prior Work and Motivation for Present Work

There has been considerable published work [1] on intersubband lasing using the III-V semiconductors InGaAs and InAlAs. An injected electron (in this case) successively transits some 25 active periods in an applied electric field and has the possiblity of emitting a laser photon in each period. This is called the Quantum Cascade Intersubband Laser (QCL) shown in figure 1. Initially , when we considered this design for our silicon-based intersubband laser operating at short wavelengths (1.6 microns), it was apparent that in order to energetically align the lower lasing level of a given period with the upper lasing level of the next period, an excessively large electric field would be required , possibly resulting in electrical breakdown. To avoid this, we considered the Quantum Parallel Laser (QPL) in which the active periods are addressed in parallel rather as a periodic superlattice. This is shown in figure 2. Population inversion has to be achieved in the QPL by bandgap engineering of a multiple well superlattice period or by using local-in-k space population inversion which arises from the nonparabolicity of the valence subbands (minibands in the case of a superlattice). Both cases will be described. It will be shown that when coupled wells are used to engineer the population inversion, the wavefunction overlap of one superlattice period to the next is too small to give sufficient

1

miniband transport for the QPL to operate satisfactorily. Hence, we focused on the local-in-k space population inversion mechanism which requires knowing (calculating) the in-plane energy dispersion to see if the nonparabolicity is sufficient for this mechanism to work.

1.2 Early models of Inplane Dispersion

Previous work showed that the quantum parallel interminband laser in which each active region consists of coupled quantum wells will not perform satisfactorily. This is shown in figure 3. Here the well and barrier widths are adjusted so that the lifetime of the upper lasing level is longer than the lifetime of the lower lasing level. This can be engineered because the lifetimes depend on the wavefunction overlap which can be varied by changing the width of the barrier between the active wells. The reason that this structure cannot act a superlattice is that the internal barriers within each active region, which are required to bandgap engineer the subband lifetimes, also severely decrease the wavefunction overlap from one active period to the next; this kind of 'lifetime engineering' is required in silicon-based structures since the transition rates are independent of momentum transfer as in the III-V's. A publication resulting from this study is reference 2, Photonics Technology Letters, May 1997, and is reproduced in Appendix A.

A more tightly coupled superlattice with larger wavefunction overlap and wider minibands is needed. One potential candidate is the ATT InGaAs/InAlAs quantum cascade laser (QCL)which does not achieve 'global' population inversion, but only 'local-in-k-space' population inversion [3]. A necessary (though not necessarily sufficient) condition is that there be enough band nonparabolicity that the emitted photon cannot be reabsorbed along the in-plane dispersion curve except at $k_x=0$. Thus, for $k_x \neq 0$, the intersubband energy difference must differ from the photon energy by more that the linewidth of the upper level, see figure 4. This mechanism requires only a single quantum well and barrier per superlattice period and so has the potential of providing sufficient interperiod electronic overlap and wide enough minibands for coherent transport. The modeling has to determine whether the interactions among the valence HH and LH bands gives rise to sufficient band nonparabolicity for this mechanism to work, and the band mixing as a function of in-plane momentum to obtain the optical phonon emission rate.

Our progam was to study that mechanism initially for the Ge_xSi_{1-x} /Si QPL to determine whether there is sufficient in-plane nonparabolicity for this mechanism to work, and , if so, to determine the nonparabolic energy dispersion and the admixture of light hole and heavy hole wavefunctions as a function of k_x. The last item is important because the initial excited state is at $k_x=0$ and is therefore entirely heavy-hole like. By emitting an optical phonon to a final state with $k_x \neq 0$, the latter is an admixture of heavy-hole and light-hole states. Since the electron-phonon interaction between states with different Bloch functions is small, the lifetime of the upper level will be increased if there is a large admixture of light-hole wavefuction in the final state, enhancing the possibility of population inversion.

2

For the Ge_xSi_{1-x} /Si QPL, our procedure was as follows: To model the in-plane dispersion, we used the 6 band (k.p) secular determinant of People and Sputz [4]. This includes all interactions in the valence band and only neglects possible interactions with the conduction band. Specifically, the secular equation for the energy eigenvalues is

$$H_E[-S_E L_E + (D/2^{1/2} - 2^{1/2}e)^2] + |a|^2[(3/2)H_E + (1/2)L_E + S_E - (D-2e)]$$

$$+|b|^2[2L_E + S_E + 2D - 4e] + 3^{3/2} Re[(a)^2b] = 0, \tag{1}$$

where

$$H_E = H-E, \quad L_E = L-E, \quad S_E = S-E,$$

$$H = H_{hh} + e, \quad L = H_{lh} - e, \quad S = 1/2(L+H)-D,$$

$$H_{hh} = -h^2/2m_0[(k_x^2 + k_y^2)(g_1 + g_2) + k_z^2(g_1 - 2g_2)],$$

$$H_{lh} = -h^2/2m_0[(k_x^2 + k_y^2)(g_1 - g_2) + k_z^2(g_1 + 2g_2)],$$

$$a = 3^{1/2}h^2/m_0[k_z(k_x - ik_y)g_3],$$

$$b = 3^{1/2}h^2/2m_0[(k_x^2 - k_y^2)g_2 - 2ik_xk_yg_3],$$

$$D = (H_{hh} - H_{lh}), \tag{2}$$

E is the eigen-energy, e is the strain energy, h is Planck's constant, the g_i are the Luttinger inverse effective mass parameters, D is the spin-orbit splitting, and the other symbols have their usual meanings.

The confinement wavevector k_z is determined from the solution in the growth (z) direction using appropriate values of the perpendicular effective masses m_z in the well and barrier. Initially, for particular values of germanium composition x, zone center ($k_x=0$) effective masses were used to obtain the confinement energies and the corresponding wavevectors $k_z(well)=[2m_{well}E/h^2]^{1/2}$ and $k_z(barrier)=[2m_{barrier}(V_{offset}-E)/h^2]^{1/2}$. For these latter values, in-plane dispersion was then calculated as a function of k_x. While the dispersion of HH1 appeared plausible, that of HH2 had a large negative hole mass which seemed unphysical. One possible error is the assumption that m_z of the well and barrier remain constant with increasing k_x. The procedure was then modified as follows:

3

(1) Values of k_z(well) and k_z(barrier) corresponding to k_x=0 were taken,

(2) A value of $k_x \neq 0$ is chosen,

(3) Values of m_z(well) and m_z(barrier) are computed from the People Sputz dispersion relation[4] using the finite difference approximation to the second derivative of E with respect to k_z for the given value of k_x and the values of k_z(well) and k_z(barrier) of step (1),

(4) Confinement energies are calculated for these values of m_z(well) and m_z(barrier) and corrected values of k_z(well) and k_z(barrier) are obtained,

(5) Steps (3) and (4) are iterated to convergence,

(6) The energy is then $E=E(k_x,k_z)$, where k_x is the value chosen in step(2) and k_z is obtained from step (5).

Though producing some changes in the in-plane dispersion, this procedure did not correct the difficulties described above.

1.3 Studies of GaAs/Al$_y$Ga$_{1-y}$As Quantum Wells

In view of the above difficulties in fitting the in-plane dispersion of Ge$_x$Si$_{1-x}$/Si quantum wells, we tried to obtain the in-plane dispersion of GaAs/Al$_y$Ga$_{1-y}$As quantum wells. This is a better studied material system, and results by other investigators are available. Here we took g_1=6.85, g_2=2.1, and g_3=2.9. The spin-orbit splitting of GaAs is Δ=340 meV. These quantities were assumed to be the same for the barrier. Three cases were simulated: (1) for the values of the g_i cited above, (2) using the average of g_2 and g_3; this makes the in-plane dispersion isotropic but does not give the correct confinement energies (3) neglecting the small difference between g_2 and g_3, effectively replacing g_3 by g_2. This gives isotropy and also the correct confinement energies. However, the same difficulties were found.

1.4 Bastard's Method for Calculating the Inplane Dispersion

An alternate and more successful procedure for calculating the in-plane dispersion is due to Bastard [5]. It starts with the 4x4 H$_{\Gamma8}$ Hamiltonian matrix. The heavy-hole and light-hole envelope wave functions for finite k_x are expanded in the envelope wavefunctions at k_x=0. The dimension of this matrix is [2(m+n)x2(m+n)], where m is the number of bound heavy-hole (HH) states and n is the number of bound light-hole (LH) states at k_x=0. The matrix elements are expressed in terms of the Luttinger parameters (assumed to be the same for the well and barrier), the subband energies at k_x=0, and overlap integrals and momentum matrix elements between the HH and LH envelope wavefunctions at k_x=0. The diagonalization of this matrix gives the in-plane dispersion as a function of k_x. We studied the case of Ge$_x$Si$_{1-x}$/Si. For

x=0.20, there are m=2 bound heavy-hole levels and only n=1 light-hole level, while for both x=0.25 and x=0.50, there are m=2 heavy-hole levels and n=2 light-hole levels.

We focused on the case x=0.50, since this choice leads to emission at shorter wavelengths. The latter case requires finding the eigenvalues of an 8X8 matrix which was easily done on MATHCAD. The results appear to be physically correct. The coupling pushes the HH1 curve to lower energies, while the HH2 curve is pushed to higher energies, thus increasing the HH2-HH1 energy difference. We consider this to be a more satisfactory situation than the InGaAs/AlInAs local in k-space intersubband laser, for which the conduction band nonparabolicity decreased the intersubband energy difference with increasing k_x. The amount of nonparabolicity appears to be sufficient for this mechanism to be viable.

We considered a QPL each period of which consists of 25 A of $Ge_{0.5}Si_{0.5}$ (well) and 15 A of Si (barrier), so the period is P=40 A. The critical thickness of the $Ge_{0.5}Si_{0.5}$ layers is 45 A for stable strain and 100 A for metastable strain; for the superlattice stack as a whole, corresponding to the average germanium content of x(avg)=0.313, the critical thicknesses are 80 A and 400 A for stable and metastable strain, respectively. So, with care, a suitable pseudomorphic superlattice of four or five periods can be grown. The heavy-hole (HH) valence band offset is 450 meV and the light-hole (LH) offset is 371 meV; the effective masses at k=0 are m_{HH} =0.240 m_0 and m_{LH} =0.178 m_0 for the well and m_{HH} =0.291 m_0 and m_{LH} =0.200 m_0 for the barrier. We solved for the energy levels of the isolated wells and then for the minbands of the superlattice. The lower HH miniband extends from 96.2 meV (at k_{sl} =0)to 117 meV (at k_{sl} =π/P), so its minibandwidth is 20.8 meV. The minimum of the upper HH minband is at 347.5 meV at the minizone boundary (k_{sl} =π/P); it is 115 meV wide and extends into the continuum above the HH barrier and has a maximum at k_{sl} =0.

Thus the tunnel injected hole relaxes to the bottom of the second miniband at the minizone boundary. Using the envelope wavefunctions for HH1,HH2, LH1 and LH2 at k_{sl} =π/P, we computed the overlap and momentum matrix elements need to obtain the in-plane dispersion. These are of the form

$$O_{HH1, LH1} = \int dz\, f_{HH1}(z)^* f_{LH1}(z), \qquad O_{HH2, LH2} = \int dz\, f_{HH2}(z)^* f_{LH2}(z),$$

$$P_{HH1, LH2} = \int dz\, f_{HH1}(z)^* [d/dz f_{LH2}(z)], \qquad\qquad (3)$$

$$P_{HH2, LH1} = \int dz\, f_{HH2}(z)^* [d/dz f_{LH1}(z)],$$

Here, the $f_i(z)$ are the k_x=0 envelope functions at k_{sl} =π/P, where k_x is the in-plane momentum.

As described in the previous section, m=2 and n=2, so the dimension of the matrix determining the in-plane dispersion is 2(m+n)x2(m+n) =8x8. The matrix appears explicitly in figure 5.

In Figure 5,

$$c_{HHi, LHj} = c(k_x, k_y)O_{HHi,LHj} \quad (i,j=1,2),$$

$$b_{HHi, LHj} = b(k_x, k_y)P_{HHi,LHj}, \quad (i,j=1,2),$$

$$c(k_x,k_y) = 3^{1/2} E_0 [g_2(k_x^2-k_y^2)-i2g_3k_xk_y], \tag{4}$$

$$b(k_x,k_y) = 2*3^{1/2} E_0(k_x-ik_y)g_3(-i),$$

$$E_0 = h^2/2m_0 = 3810 \ meV*A^2$$

Starting with the energies at $k_x=0$, the in-plane energy dispersion is plotted as a function of k_x for the HH1, HH2, LH1 and LH2 levels in figure 6. Also shown are the dispersion curves in the absence of interaction, denoted by '0'. It is noted that the HH1 energy is pushed to lower hole energy, increasing its effective mass in the growth (z) direction, a general result as pointed out by Bastard. On the other hand, the HH2 curve is pushed to higher energies by the interaction. Thus the energy difference between HH1 and HH2 increased with k_x, a more satisfactory kind of nonparabolicity than in the III-V InGaAs/AlGaAs where the difference decreased with k_x. The amount of nonparabolicity predicted by the above calulation appears to be sufficient for the local-in-k-space mechanism to work, though the furthur details of this mechanism have yet to be worked out. A publication of this work appeared in Journal of Applied Physics, reference [6], and is reproduced in Appendix B.

1.5 The Method of Andreani et al

The Quantum Parallel laser in the SiGe material system operates between two heavy hole minbands in the valence band. Due to the k.p interactions among the valence bands (heavy-hole, hh; light-hole, lh; split-off, so) the inplane energy dispersion $E(k_{//})$, where $k_{//}$ is the wavevector in the plane of the layer, is highly nonparabolic. Then, because the photon emitted at $k_{//}=0$ cannot be reabsorbed except at $k_{//}=0$ (due to the above nonparabolicity), the population inversion is local in $k_{//}$ space (at $k_{//}=0$) , rather than globally over the entire $E(k_{//})$ dispersion curve.

Bastard's method for calculating the inplane dispersion described in section 1.4 assumes that the Luttinger parameters of the well and barrier are the same, and , if they differ, an average is taken. Thus, his method is only approximate. Instead of the Ge_xSi_{1-x} /Si superlattice on a Si substrate, we next considered the Si/Ge strain-symmetrized short period superlattice on a Ge_ySi_{1-y} buffer layer (y=0.5 for equal thicknesses of Si and Ge). This has a number of advantages over the previoulsly described $Ge_{0.5}Si_{0.5}$ /Si superlattice on a Si substrate: First, the strains in the Si andGe layers are opposite in sign so that no integrated strain energy is accumulated for a multilayered system and ideally there is no limit on the height of the superlattice, as long as the individual layer thicknesses are below their critical thichness for pseudomorphic growth; this in not the case for the $Ge_{0.5}Si_{0.5}$ /Si superlattice on a Si substrate where a net strain energy is accumulated. Secondly, compositional rounding of the Ge concentration in the growth of the $Ge_{0.5}Si_{0.5}$ wells is avoided. This rounding distorts the shape of the quantum wellls, changing the subband energies. Thirdly, alloy scattering is avoided, leading to longer lifetimes. So, we considered the Si/Ge strain-symmetrized short period superlattice on a Ge_ySi_{1-y} buffer layer . Here it was recognized that the Luttinger parameters (and other properties) of Si and Ge are very different , so another method is required which takes these differences explicitly into account. Such a method will be especially important for future work on e.g. the Si/ZnS system where the two materials have very different properties. Such a procedure is given by Andreani, Pasquarello, and Bassani [7] . These authors exactly solve the multiband effective mass equation for the valence band envelope functions, analogous to the solution for a single parabolic band with different effective masses for the well and barrier. Imposing continuity of the multiband envelope functions and currents at the heterointerfaces leads to a 16x16 determinant which can be reduced to an 8x8 determinant by symmetry arguments. From the zeros of this determinant the inplane dispersion $E(k_{//})$ can be determined. Andreani's algorithm was programed in MATHCAD , in particular setting up and evaluating the 8x8=64 matrix elements in their secular determinant for an isolated quantum well. The authors pointed out that their method can be extended from an isolated quantum well to a periodic superlattice, but that here one must deal with the full 16x16 determinant. This extension was done at a later stage.

1.6 Calculation of Band Offsets for the Strain-Symmetrized Si/Ge Superlattice

The conduction and valence band offsets of the Ge/Si superlattice on a Si0.Ge0.5 buffer layer have been calculated following the procedure of Kahan, Chi, and Friedman [8]. The offsets of the Ge and Si layers are found with respect to the Si0.Ge0.5 buffer layer, which then determines the offsets of Si and Ge with respect to one another. The detailed procedure is as follows:

Three band model (heavy hole, light hole, split-off spin orbit band):

For both the Si and Ge layers, the average valence band energy including spin-orbit interaction and hydrostatic strain is given by

$E_{v,av}' = E_{v,av} + \Delta/3 + a_v(2-\lambda)e$,

where $E_{v,av}$ is the average valence band energy in the absence of spin-orbit and hydrostatic strain ($E_{v,av}$=-7.03 eV for Si and -6.35 eV for Ge), Δ is the spin-orbit energy (44 and 290 meV for Si and Ge, respectively), a_v is the hydrostaic deformation potential (2.4 6 and 1.24 eV), and $\lambda = 2C_{12}/C_{22}$, where C_{12} and C_{22} are the elastic constants (C_{12}= 0.650x10^{11} dyn/cm^2, 0.494x10^{11} dyn/cm^2; C_{22}= 0.801x10^{11} dyn/cm^2, 0.684x10^{11} dyn/cm^2 for Si and Ge, respectively), e is the inplane strain with respect to the $Si_{0.5}Ge_{0.5}$ buffer layer, e=+0.02 for Si (tensile strain), and -0.02 for Ge (compressive strain). We calculate $E_{v,av}'$ =-6952.7 meV for Si and -6284.3 meV for Ge. The next step is to add to these quantities the splittings due to uniaxial shear. These are[4]

$dE(hh) = e$,   (hh=heavy-hole)

$dE(lh) = -1/2(e+\Delta) + 1/2[e^2 + \Delta^2 - 2e\Delta]^{1/2}$ (lh=light hole)

$dE(so) = -1/2(e+\Delta) - 1/2[e^2 + \Delta^2 - 2e\Delta]^{1/2}$ (so= split-off)

We calculate   dE(hh) = -77.6 mev, dE(lh) = +142.27 meV, dE(so) =-108.66 meV for Si and dE(hh) = 100 mev, dE(lh) =-24.61 meV, dE(so) =-365.44 meV for Ge. Finally, Ev(i) = Ev'+ dE(i), where i=hh,lh,so. We obtain
Ev(hh)=-7030.3 meV, Ev(lh)=-6810.43 meV, Ev(so)=-7061.36 meV for Si and

Ev(hh)=-6184.3 meV, Ev(lh)=-6308.91 meV, Ev(so)=-6649.74 meV for Ge. The valence band offsets of Ge/ Si are then
V(hh) = Ev(hh, Ge)- Ev(hh, Si)= 836 meV, V(lh) = Ev(lh, Ge)- Ev(lh, Si)= 501.5 meV,
V(so) = Ev(so, Ge)- Ev(so, Si)= 411.62 meV,

The band alignment is type II, holes are confined to the Ge layers and electrons to the Si layers.

Two band model (heavy hole, light hole):

Models for calculating the inplane dispersion use only the heavy and light holes, and the split-off spin orbit band is neglected. So, to be consistent, the offsets should be obtained for the two band case. This is obtained from the three band case by letting the spin-orbit splitting $\Delta \rightarrow \infty$, i.e. making the split-off band infinitely remote. We then obtain
dE(hh) = -77.6 mev and dE(lh) = +77.6 meV for Si, and dE(hh) = 100 mev,
dE(lh) = -100 meV for Ge, so that
Ev(hh)=-7030.3 meV, Ev(lh)=-6875.1 meV for Si and
Ev(hh)=-6184.3 meV, Ev(lh)=-6384.3 meV for Ge.
So for the two band model, the valence band offsets are V(hh) = Ev(hh, Ge)- Ev(hh, Si)
= 836 meV,

V(lh) = Ev(lh, Ge)- Ev(lh, Si)= 490.8 meV,
V(hh) is the same and V(lh) not much different from the three band case.
The results are shown in Figure 7.

1.7 Analysis of the Strain-Symmetrized Si/Ge Superlattice for Intersubband lasing

As previously discussed , the strain-symmetrized Si/Ge superlattice on a Si0.Ge0.5 buffer layer (on a Si substrate) has a number of advantages over the previously described Si0.Ge0.5 /Si superlattice quantum parallel laser diode. First, the strains in the Si and Ge layers are opposite in sign so that no integrated strain energy is acquired for a multilayered system and ideally there is no limit on the height of the superlattice; this is not the case for the Si0.Ge0.5 /Si system. Secondly, compositional rounding of the Ge concentration in the growth of the Si0.Ge0.5 alloy layers is avoided. This rounding distorts the shape of the quantum wells, changing the subband energies. Thirdly, alloy scattering is avoided. leading to longer lifetimes. We are therefore investigating the strain symmetrized Si/Ge system rather than the alloy system.

Summary of Results: A unipolar p-i-p silicon-based intersubband laser consisting of a symmetrically strained Ge-Si superlattice on a relaxed Si0.5 Ge0.5 buffer layer was modeled and analysed. The strain-symmetrization removes the limitation on the size of the superlattice.

Analysis of the in-plane energy dispersion shows that the population inversion is local-in-k-space. For a 11ML/11 ML superlattice (15.4 A/15.4 A), interminiband lasing between HH2 and HH1 is predicted at λ= 2.26 mm. From the envelope functions and material properties, the minband lifetimes and laser gain are calculated. For a current density of 10000 A/cm^2, a gain of G_L= 96 cm^{-1} was calculated

In section (1.4), simulations of a p-i-p coherently strained Si0.5 Ge0.5/Si superlattice laser were presented. Calculations were made of the local-in-k-space population inversion between the nonparabolic heavy-hole valence subbands, HH1 and HH2. Lasing was predicted at λ= 5.4 mm with a lifetime difference of 2.4 ps. Here we present a similar study for the symmetrically strained Si/Ge superlattice grown on a Si0.5 Ge0.5 buffer layer. However, this system has several advantages over the Si0.5 Ge0.5/Si superlattice laser. First, since no integrated strain is accumulated in the structure, there is no limitation on the size of the superlattice as long as the individual layer are below their critical thicknesses. In addition, compositional rounding of the Ge concentration is avoided , the structures are simpler to grow, and alloy scattering is eliminated. Furthur, the Si/Ge superlattice has large band offsets so that lasing wavelengths in the mid to near infrared are possible. Specifically, we propose a superlattice structure with equal layer thicknesses of Si and Ge layers [11 monlayers (ML)/11 (ML) ; 15.4 A/ 15.4 A] on a Si0.5 Ge0.5 buffer layer grown on a Si substrate. The Ge layers are under 2% compressive strain and the Si layers under 2% tensile strain. By calculating the band offsets with respect to the substrate, the band offsets of the Ge and Si layers with respect to one another are obtained. The band alignment is type II, with holes tending to be in the Ge layers and electrons in the Si layers. For a unipolar p-i-p structure, hole transport occurs in the Ge wells confined by Si barriers. As shown above, the heavy-hole valence band offset at $k_{/\!/}$=0 is found to be V_{HH} =836 meV and the light hole offset V_{LH} =501 meV, where $k_{/\!/}$ is the inplane crystal momentum. The bandedge energy diagram is shown in figure 7 , where the conduction band offsets are deduced from earlier work by Abstreiter et al. This superlattice gives rise to two heavy-hole (HH) minibands. The lowest (HH1) is centerred at 252 meV above the heavy-hole band edge in the Ge wells and is 24 meV wide, sufficient for miniband transport rather than incoherent hopping. The next higher heavy-hole miniband (HH2) is centerred at 930 meV and is 228 meV wide, extending into the continuum. Between these is the light-hole miniband (LH1) extending from 300 to 400 meV with respect to the heavy-hole band edge.

Because of the interaction of the minibands, the inplane energy dispersion is highly nonparabolic. Specifically, the energy difference between HH1 and HH2 increases with increasing inplane wavevector k_x. As first shown for the InGaAs/InAlAs system, the photon emitted at $k_{/\!/}$=0 cannot be reabsorbed at finite $k_{/\!/}$ if the energy difference exceeds the photon energy by more than the line width of the upper level. The population inversion is not over the entire minbands but is only local in k-space (at $k_{/\!/}$=0). It follows from that fact that the optical phonon mediated intersubband lifetime (HH2-HH1) is longer than the intrasubband lifetime (HH1-HH1). In addition, the effective lifetime of the lower state is decreased by the probability that the hole will tunnel to the collector. Because of the large energy difference in the present example, some 12 intrasubband cascades are required to reach the vicinity of $k_{/\!/}$=0

and it may tunnel at each cascade. Thus the effective lower state lifetime is reduced considerably.

Since the Luttinger parameters of Ge and Si are quite different, the inplane energy dispersion was calculated by the method of Andreani et al [7]. Though their method can be generalized for a superlattice, we consider an isolated Ge quantum well surrounded by Si barriers. An outline of their procedure is as follows: Starting from the 4X4 Luttinger Hamiltonian, the bulk hole dispersion is found for the light and heavy holes. For a given value of the inplane momentum $k_{//}$ and energy E, the corresponding wavevectors for the light and heavy holes, $kz=k_l(E)$ and $k_h(E)$, are found. Next, from the continuity of the four component wavefunctions and currents at the well and barrier interface $z=L/2$, an 8X8 determinent is obtained in which the previously obtained values of $k_l(E)$ and $k_h(E)$ are substituted. The zeros of the determinant $D(E, k_{//})$ give the eigenvalues E for the given value of $k_{//}$. In practice, $D(E, k_{//})$ is plotted as a function of E to locate the approximate position of its zeros and then a search determines where $D(E, k_{//}) =0$.

Miniband Transport

For the Ge well, the Luttinger parameters are $g_{1w}=13.4$, $g_{2w}=4.25$, $g_{3w}=5.69$, while for the Si barrier, $g_{1b}=4.22$, $g_{2b}=0.39$, $g_{3b}=1.44$. The Ge wells are under 2% compressive strain with respect to the buffer layer and the strain energy is calculated to be 100 meV. The heavy hole bandedge lies above that of the light hole bandedge at $k_{//}=0$ by this amount. Similarly, the Si barriers are under 2% tensile strain with a strain energy of -77 meV, the light hole edge lying above that of the heavy hole edge by 77 meV. Taking these uniaxial splittings into account, the heavy-hole valence band offset at $k_{//}=0$ is found to be $V_{HH} =836$ meV and the light hole offset $V_{LH} =501$ meV. The inplane dispersion of HH1 is repelled toward positive energies by an amount sufficient to render the population inversion local in k space. We consider a strain symmetrized superlattice with well (Ge) and barrier (Si) widths of 15.4 A . Simulating the perpendicular transport for the heavy holes ($m_w=0.2$ m_0 , $m_b=0.291$ m_0, $V_{HH}= 836$ meV), we obtain a lower heavy hole miniband (HH1) extending from 246 meV at $k_{sl}=0$ to 270 meV at the minizone boundary at $k_{sl}=\pi/P$, where P is the superlattice period. The minimum of the upper heavy hole miniband (HH2) is at 827 meV at $k_{sl}=\pi /P$, just below the barrier, and extends into the continuum. The optical (lasing) transition occurs at $k_{sl}=\pi/P$, the emitted photon having an energy of 547 meV corresponding to a wavelength of $\lambda= 2.26$ μm. The much stronger nonradiative process is the emission of a nonpolar optical phonon to a state of finite inplane momentum on the lower miniband (HH1). From this state, the hole cascades down to the minimum at $k_{sl}=0$ by sequentially emitting optical phonons. As previously discussed, since the hole cannot reabsorb the emitted photon, it can only cascade down or tunnel to the collector.

11

To calculate the intersubband transition rate and therefore the lifetime of the upper state, we need to know the envelope wavefunctions $|i>$ and $|j>$ at $k_{sl}=\pi/P$ from which we can calculate the overlap or interference factor

$$G_{ij}(q_z) = <i \mid \exp(i\, q_z\, z)|j>,$$

where q_z is the phonon wavevector in the z (growth) direction. Then with

$$I_{ij} = \int dq_z\, G_{ij}(q_z),$$

the intersubband scattering rate due to emisssion of an nonpolar optical phonon is given by

$$Wij = [m_{HH}\, D_0\, /\, 4\pi\rho h(h\omega_{op})]\, [n(h\omega_{op})+1]I_{ij}$$

where $m_{HH}=0.2\, m_0$ is the heavy hole mass in the well, $D_0=8.7\times108$ eV/cm is the optical deformation potential, $\rho=5.32$ gm/cm3 is the mass density $h\omega_{op} = 37$ meV is the optical phonon energy of Ge, and

$$n(\omega_{op})=[\exp(h\omega_{op}\,/kT)-1]^{-1}$$

is the number of phonons of energy $h\omega_{op}$. Although the intersubband transition is a large wavevector transition, we neglect the dispersion of the phonon frequency and take ω_{op} to be a constant (Einstein approximation); this should introduce only a small error. We calculate at room temperature

$$Wij = 1.05\times10^{13}\, A\, sec^{-1}\, Iij$$

For the above intersubband transition, we find that $I_{21}=0.0629$ A^{-1}, while for the intrasubband transition $I_{11}=0.1758$ A^{-1}. Thus the lifetimes are

$$t_{21} = W_{21}^{-1} = 1.515\ psec,\ and\ t_{11} = W_{11}^{-1} = 0.54\ psec$$

Thus population inversion is established due to the fact that the intrasubband scattering rate is larger than the intersubband rate. In addition, there is another factor which leads to a larger disparity in these rates, namely, phonon confinement. Specifically, there is a large difference is the bulk optical phonon frequencies of the well and barrier [$v_{op}(Si) = 15.5$ THz, $v_{op}(Ge) = 9$ THz], and as a result, the optical phonons tend to be confined. Earlier studies[9]of phonon confinement for the SiGe/Si heterosystem showed that the intersubband rate was reduced by approximately a factor of 3 with respect to bulk phonons while the intrasubband rate was increased by a factor of approximately 2. Applying these correction factors, we obtain

$t_{21}' = (W_{21}')^{-1} = 4.54$ psec, and $t_{11}' = (W_{11}')^{-1} = 0.27$ psec

As stated above, at each downward intrasubband cascade, the hole may tunnel to the collector. To obtain the probability that the hole reaches the bottom of the miniband, we need the tunnel rate to the collector which we consider next.

Tunneling Rate

In this section, the tunnel rate form the lower miniband to the collector is calculated. The centroid of the lower miniband is at 268 meV above the heavy hole band edge. The heavy hole offset is V=836 meV, the heavy hole mass of the Ge well is m_w=0.2m_0, the mass of the Si barrier is
m_b= 0.291m_0, and we choose the width of the barrier to be 5 monolayers (7 A). Then with

$E_0 = 3810$ meV A^2

$k(E) = [(E/E_0) \, m_w]^{1/2}$, $k(E,V) = [V-E)m_b/E_0]^{1/2}$

$e(E,V) = [\, k(E,V) \, m_w / \, k(E)m_b - \, k(E)m_b / \, k(E,V) \, m_w]$,

The transmission probability is

$T(E,a,V) = |exp(-i2k(E)a) / \, cosh(2k(E,V)a) + i(e(E,V)/2)sinh(2k(E,V)a)|^2$

For the above specified values of the parameters, we calculate

$T(E,a,V) = 0.189$

The mean group velocity of the lower miniband is $v = \Delta E \, P/2h$,

where ΔE=24 meV is the width of the lower miniband and P=30.8 A is the period. This gives

$v = 5.6 \times 10^6$ cm/sec.

Choosing 10 periods, the time for a hole to transit the structure is

$t_{tr} = 0.55$ psec

The tunelling rate is

$$W_{tun} = (1/ t_{tr}) \, T(E,a,V)$$

We calculate

$$W_{tun} = 0.35 \text{ psec}^{-1}, \; t_{tun} = (W_{tun})^{-1} = 2.9 \text{ psec}.$$

At each intrasubband cascade, the probability that the hole will not have tunneled to the collector is

$$W_{intra} / (W_{intra} + W_{tun}) = t_{tun} / (t_{tun} + t_{intra}) = 0.91$$

If we take 10 cascades, the effective lifetime of the lower state is

$$t_l = (0.91)^{10} \, t_{tun} = 1.16 \text{ psec},$$

while the previously calculated lifetime of the upper level is

$$t_U = 4.54 \text{ psec.}$$

Laser Gain

The gain is

$$G_L = \sigma_{ul} \, (Nu - Nl),$$

where the cross section

$$\sigma_{ul} = (4\pi a_0/n_0)(E_L / \Gamma) \, |z_{ul}|^2,$$

where $a_0 = 1/137$ is the fine structure constant, $n_0 = 3.5$ is a mean index of refraction, $E_L = 547$ meV is the lasing energy, and Γ is the linewidth of the upper level at $k_{sl} = \pi/P$; we choose $\Gamma = 10$ meV. Finally,

$$z_{ul} = \int dz f_u(z) z f_l(z)$$

is the optical dipole matrix element, where $f_u(z)$ and $f_l(z)$ are the envelope functions at the minizone boundary $k_{sl} = \pi/P$ of the upper and lower levels, respectively. We obtain $z_{ul} = 1$ A. We comment on the small magnitude of z_{ul} later. The population difference $(N_u - N_l)$ between the upper and lower states is found from a rate equation analysis of the effective two level system:

$(N_u - N_l) = (J/e)t_U [1 - t_l] / t_U],$

where J is the current density and e is the electronic charge. We calculate

$(N_u - N_l) = 3.4 \times 10^{17}$ cm^{-3} and

$G_L = 96$ cm^{-1} for a current density of J = 10000 A cm^{-2}; of course the gain G_L scales directly with J.

1.8 Asymmetric Strain-Symmetrized Ge/Si Interminiband Laser

Summary: We present quantum-mechanical analysis of a proposed Si-based Ge/Si superlattice p-i-p laser diode grown upon a relaxed Si$_{0.25}$Ge$_{0.75}$ buffer layer. Local-in-k-space population inversion between hh2 and hh1 minibands at the SL minizone boundary is predicted for the 4.6 um lasing wavelength. Although the 2.94 nm quantum well width is three times the 0.98 nm Si barrier width, the superlattice has net zero strain. A large dipole matrix element |Z21| = 5.7 A is calculated, leading to an expected gain of 238 cm-1 at 3 kA/cm2 injection current density.

In the previous section (1.7), we analyzed a unipolar p-i-p strain-symmetrized Ge/Si interminiband laser on a relaxed Si$_{0.5}$Ge$_{0.5}$ buffer layer. Due to the strong valence band nonparabolicity, the population inversion is local in k-space. With the Si$_{0.5}$Ge$_{0.5}$ buffer layer, the well and barrier dimensions are constrained to be equal (W = B) to insure strain symmetrization . For a 11 ML/11 ML (15.4A/ 15.4A) superlattice, lasing was predicted at λ=2.2 im. However, a small dipole matrix element $z_{21} = 1$ A was obtained resulting in a concomittant small laser gain of $G_L = 96$ cm^{-1} at a current density of 10 kA/cm^2. In this section, an added degree of freedom is gained by considering a variable composition buffer layer and unequal well and barrier widths while maintaining overall strain-symmetrization. Specifically, we consider a Ge-rich Si$_{0.25}$Ge$_{0.75}$ buffer and a B/W =7ML/21ML (9.8A/ 29.4A) superlattice. The wider wells (W=3B) results in a smaller interminiband photon energy, but a larger dipole matrix element is obtained, $| z_{21}| = 5.7$ A; this is significant since G_L is proportional to $| z_{21}|^2$. Here the lasing wavelength is λ= 4.6 im and we calculate a gain of $G_L = 238$ cm^{-1} for a current density of only 3 kA/cm^2.

Miniband Stucture and Lasing Transition

The band diagram of our proposed type-II superlattice is shown in figure 8. The valence band offsets were obtained by the procedure of Kahan et al [8] which in turn follow the procedure of Van de Waal [10]. For the Si$_{0.25}$Ge$_{0.75}$ buffer layer, the Si barrier layers are under 3% tensile strain and the Ge well layers are under 1% compressive strain. The previously described procedure gives the following valence band offsets of the Ge layers with respect to the Si: $V_{HH} = 819$ meV, $V_{LH} = 486$ meV.

15

The location at $k_{//}=0$ ($k_{//}$ is the inplane momentum) of the heavy-hole (HH) minibands is obtained using $V_{HH} = 819$ meV, $m_W = m_{Ge} = 0.206\ m_0$, $m_B = m_{Si} = 0.291\ m_0$, where m_0 is the free electron mass. The lower HH1 miniband extends from 99 meV to 121 meV, 22 meV wide, which is sufficient for coherent transport. The upper HH2 minband extends from 389 meV to 487 meV, 98 meV in width. The optical (lasing) transition occurs at the minzone boundary $k_{sl} = \pi/P$ (P=W+B is the superlattice period) and at $k_{//}=0$. The energy of the emitted photon is 268 meV, corresponding to a wavelength of $\lambda = 4.6$ im.

Nonradiative Processes

The most rapid nonradiative transition is due to the emission of a nonpolar optical phonon
(acoustical phonon emission is slower by two to three orders of magnitude). The optical phonon energy of Ge is $\hbar\omega_{opt} = 37$ meV. Now although the 268 meV energy difference at $k_{//}=0$ far exceeds $\hbar\omega_{opt}$, the optical phonon can be emitted by making a transition from HH2 to HH1 at a finite value of $k_{//}$. The inplane dispersion of the superlattice at the minzone boundary $k_{sl} = \pi/P$ was obtained by extending the method of Andreani et al [7] to a superlattice. The result is shown in figure 8 . The departure from nonparabolicity of HH1 and HH2 is clearly sufficient for the local-in-k-space mechanism to be operative. In addition to the two heavy-hole bands, the intervening light-hole band is shown. As explained earlier, the light- hole miniband does not seriously affect the transition HH2 to HH1.

The procedure for obtaining the minband lifetimes was given earlier. For the intersubband lifetime we calculate $t_{21}'' = 1.34$ psec and for the intrasubband lifetime $t_{11}' = 0.72$ psec, so that
$t_{21}'' > t_{11}''$ as required for population inversion. Taking into account the effect of phonon confinement as explained , we get $t_{21}' = 4$ psec and $t_{11}' = 0.36$ psec. Holes occupying the lower miniband exit to the collector by tunneling through a narrow (4 ML=5.6 A) Si barrier. Tunneling can occur at each step as the hole cascades by sequentially emitting optical phonons. A tunneling time 3 psec was calculated and six cascades are required. To obtain the effective tunnel lifetime , the tunnel time must be multiplied by the probability of the hole reaching the bottom of the lower miniband. Following this procedure, the lifetimes of levels 2 and 1 are found to be $t_2 = 4$ psec and $t_1 = 1.5$ psec. We take a steady current density of J= 3000 A/cm^2 and assume a linewidth of $\Gamma = 10$ meV for the upper level 2 at $k_{sl} = \pi/P$. We calculate a population difference $\Delta N = N_2 - N_1 = 1.2 \times 10^{17}$ cm^{-3} and a laser gain of $G_L = 238$ cm^{-1}.

For the proposed quantum-parallel laser , the emitter contact is a pseudomorphic p-Si$_x$ Ge$_{1-x}$ alloy layer with x chosen such that it's quasi-Fermi level is just above the bottom of the HH2 miniband. To determine the Ge composition x of the emitter, the bandedge of the strained Si$_x$ Ge$_{1-x}$ alloy was calculated with respect to the Si$_{0.25}$Ge$_{0.75}$ buffer. The physical paramenters of the alloy were found by interpolation. It was found that for x=0.55, the valence bandedge of

the emitter alloy is 6 meV above the bottom of the upper miniband and, if heavily doped p-type, is suitable for hole injection through a thin Si tunnel barrier. The tensile strain is only 0.8% with respect to the buffer layer, so the emitter can be a few hundreds of angstroms thick and therefore bulk-like. Similarly, x of the pseudomorphic p- $Si_x Ge_{1-x}$ collector contact is chosen so that the bottom of the HH1 lower miniband is just above the collector's quasi-Fermi level. For x=0.932 (nearly pure Ge), the collector valence band edge is an optical phonon energy (37 meV) below the bottom of the lower miniband, thereby facilitating hole transfer from the lower miniband to the collector. The collector is under 0.7% compressive strain. A perspective view of the proposed Fabry-Perot laser resonator is shown in figure 9.

Conclusion: Assuming that pure Ge and Si layers are used for the active superlattice of a short-period quantum-parallel laser, we find that an imbalance of tensile and compressive strain between well and barrier adds a useful degree of freedom for optimization of the laser matrix element. Unequal strain is produced by making the buffer composition different from $Si_{0.5}Ge_{0.5}$, and if the ratio W/B is made inverse to the strain ratio, the resulting SL has zero overall strain. For a $Si_{0.25}Ge_{0.75}$ buffer, we calculate a 5.7x increase in $|z_{21}|$, an 8x gain enhancement, and a 2.1x increase in lasing wavelength.

17

1.9 References

(1) J. Faist, F. Capasso, D.L. Sivco, A. L. Hutchinson, and A. Y. Cho, Science **264** , 553 (1994)

(2) L. Friedman and R.A. Soref, IEEE Photonics Technology Letters, **9**, No. 5 (1997)

(3) J. Faist, F. Capasso, C. Sirtori, D.L. Sivco, A. L. Hutchinson, M.S. Hybertsen and A. Y. Cho, Phys. Rev. Lett., **76**, No. 3 (1996)

(4) R. People and S.K. Sputz, Phys. Rev. B **41**, 8341 (1990)

(5) G. Bastard, " Wave Mechanics Applied to Semiconductor Heterostructures", Les Editions de Physique, p.108 (1990)

(6) L. Friedman and R.A. Soref, Journal of Appl. Physics **83** , No. 7, p. 3480 (1998)

(7) L.C. Andreani, A. Pasquarello, and F. Bassani, Phys. Rev. B **36** , p. 5887 (1987)

(8) A. Kahan, M. Chi, and L. Friedman, Journal of Appl. Physics **75**(12), p. 8012 (1994)

(9) G. Sun and L. Friedman, Phys. Rev. B **53** No. 7 , p. 3966 (1996)

(10) C. G. van de Walle and R. M. Martin, Phys. Rev. B **34** , 5621 (1986)

1.10 FIGURES
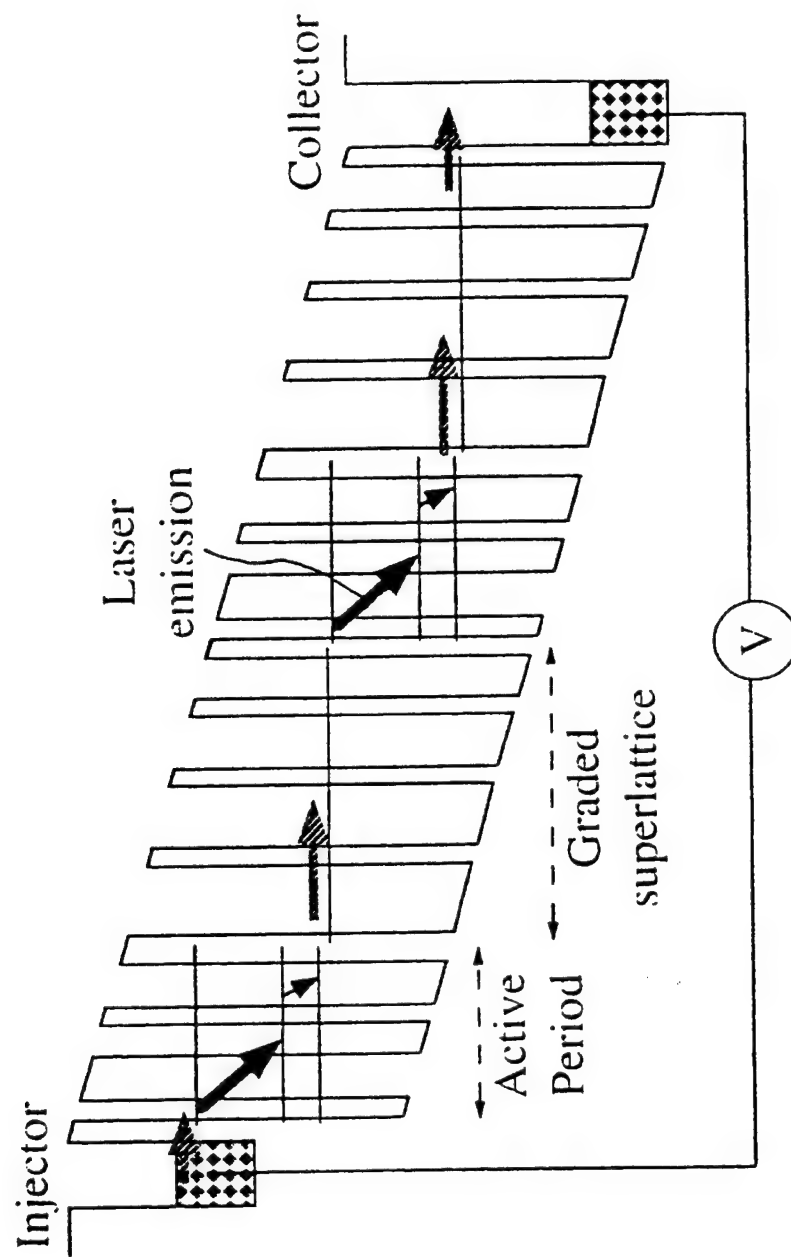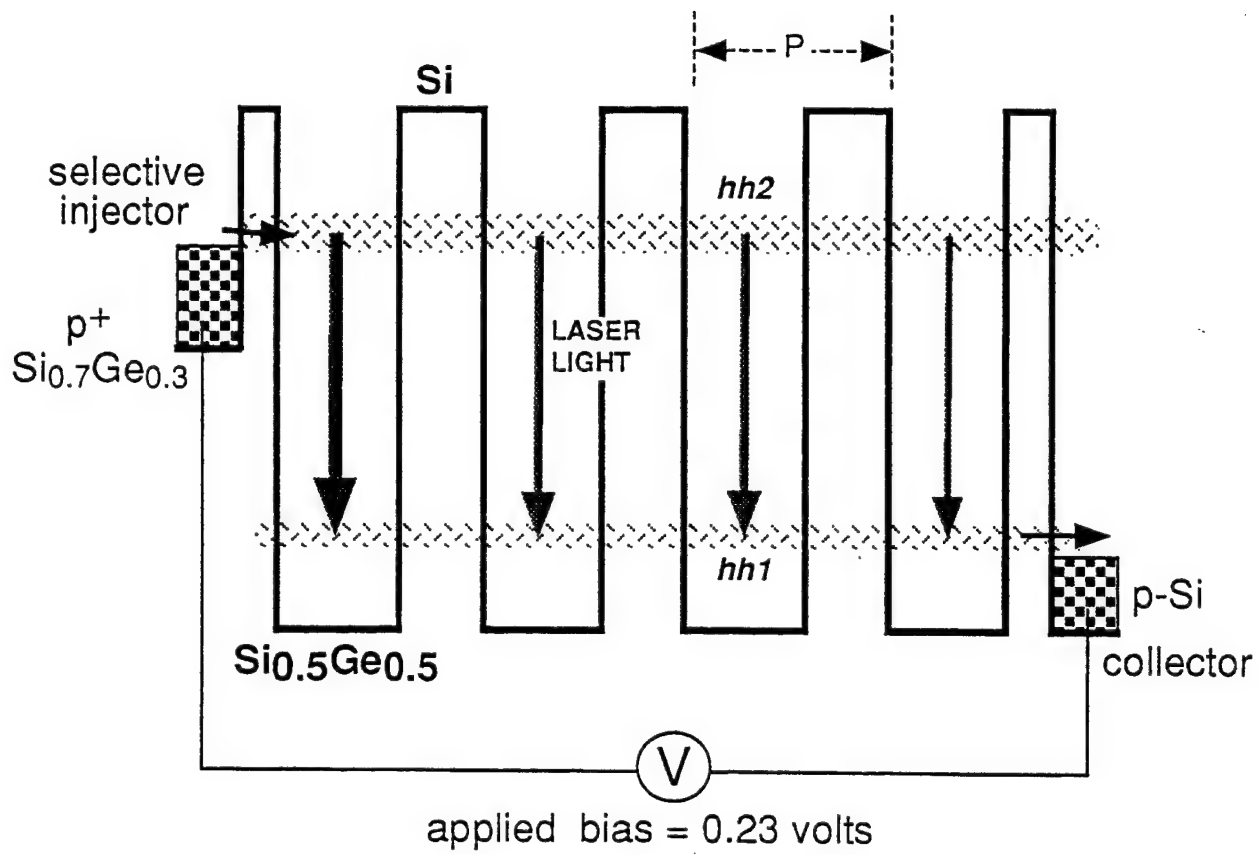
Injector

Collector

Laser emission

Active Period

Graded superlattice

V

20
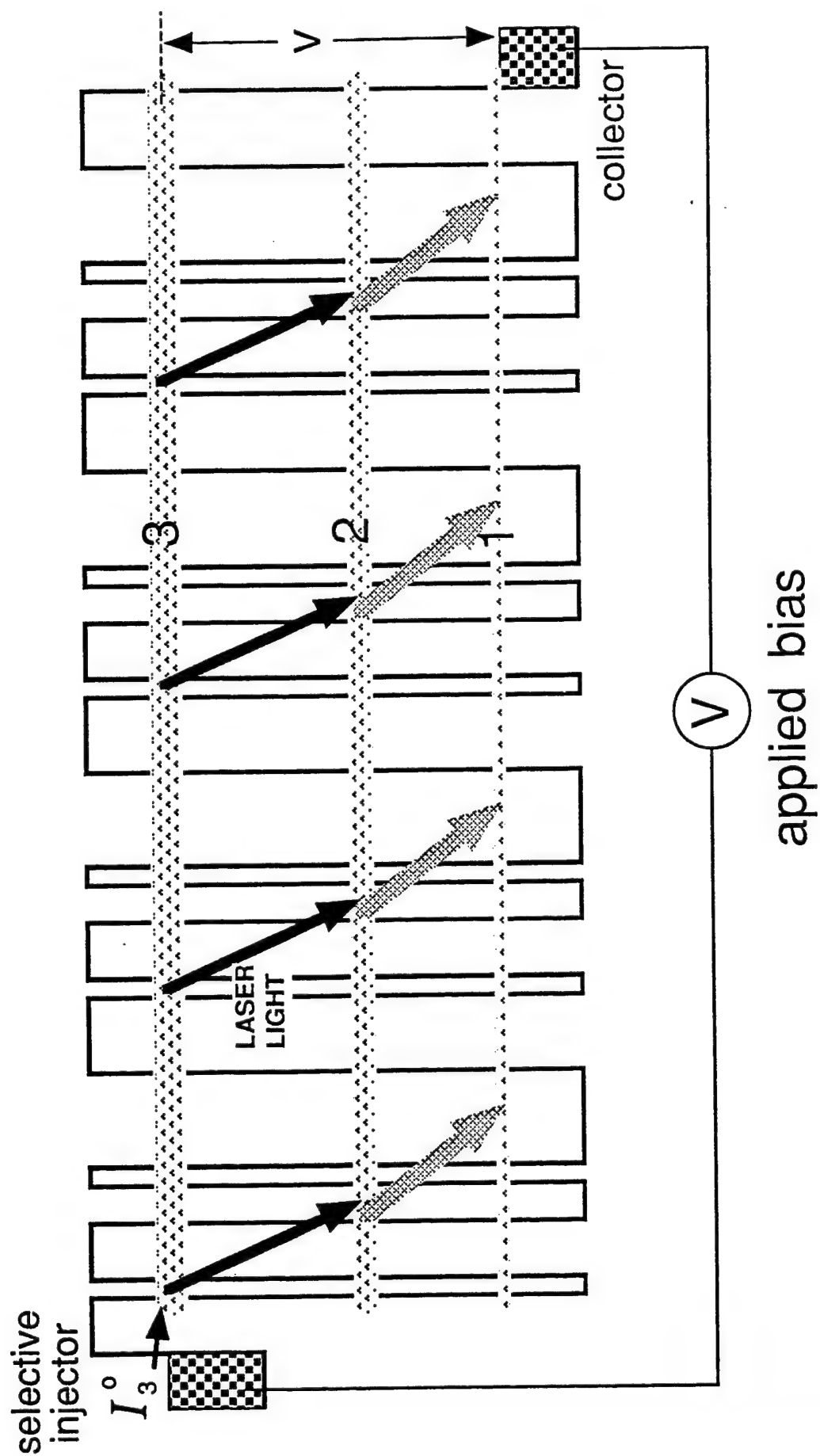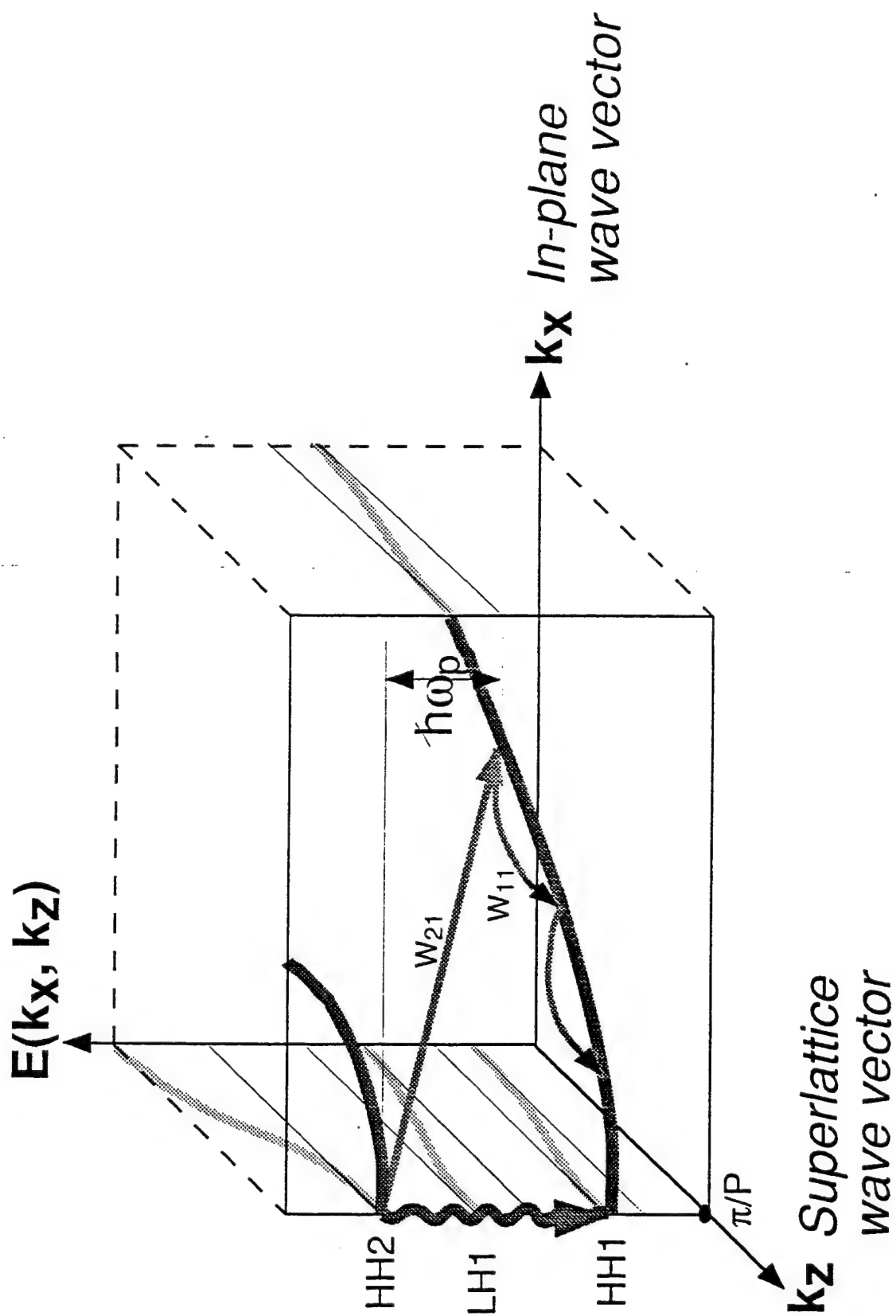
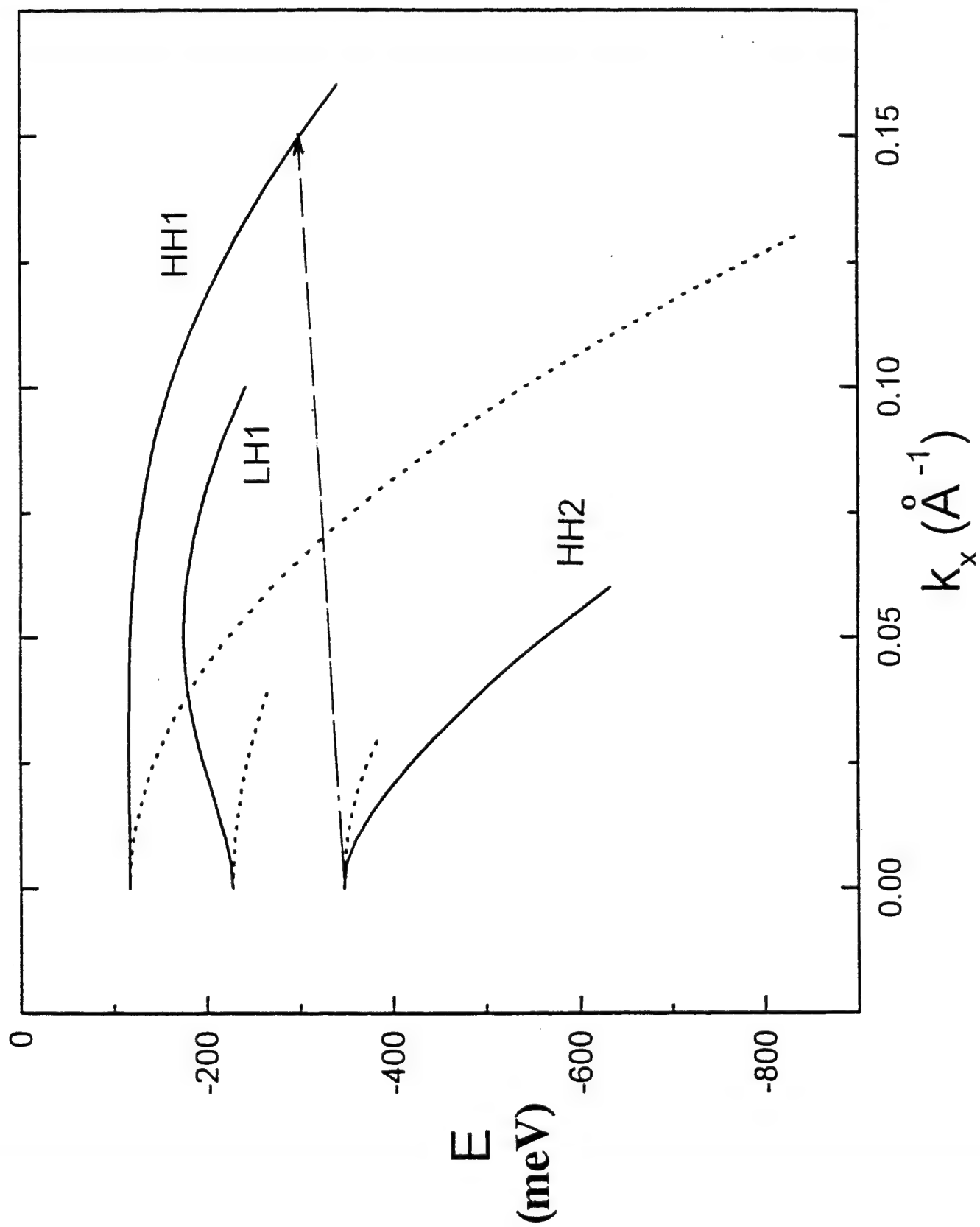The quantum-parallel laser: p+-i-p diode showing lasing between two valence mini-bands of $Si_{0.5}Ge_{0.5}/Si$ superlattice.

Local-in-k_x population inversion within the $Si_{0.5}Ge_{0.5}$ quantum wells of Fig. 1. Diagram shows in-plane dispersion of valence subbands at superlattice mini-zone boundary.

$$M(k_x,k_y,\zeta,E) =$$

$$
\begin{bmatrix}
E_{HH1}(k_x,k_y) - E & 0 & c_{HH1LH1}(k_x,k_y,\zeta) & 0 & 0 & b_{HH1LH2}(k_x,k_y,\zeta) & 0 & 0 \\
0 & E_{HH2}(k_x,k_y) - E & 0 & c_{HH2LH2}(k_x,k_y,\zeta) & b_{HH2LH1}(k_x,k_y,\zeta) & 0 & 0 & 0 \\
c_{LH1HH1}(k_x,k_y,\zeta) & 0 & E_{LH1}(k_x,k_y) - E & 0 & 0 & 0 & 0 & 0 \\
0 & c_{LH2HH2}(k_x,k_y,\zeta) & 0 & E_{LH2}(k_x,k_y) - E & 0 & 0 & -b_{LH2HH1}(k_x,k_y,\zeta) & -b_{LH1HH2}(k_x,k_y,\zeta) \\
0 & b_{LH1HH2}(k_x,k_y,\zeta) & 0 & 0 & E_{LH1}(k_x,k_y) - E & 0 & c_{LH1HH1}(k_x,k_y,\zeta) & 0 \\
b_{LH2HH1}(k_x,k_y,\zeta) & 0 & 0 & 0 & 0 & E_{LH2}(k_x,k_y) - E & 0 & c_{LH2HH2}(k_x,k_y,\zeta) \\
0 & 0 & 0 & -b_{HH1LH2}(k_x,k_y,\zeta) & c_{HH1LH1}(k_x,k_y,\zeta) & 0 & E_{HH1}(k_x,k_y) - E & 0 \\
0 & 0 & -b_{HH2LH1}(k_x,k_y,\zeta) & 0 & 0 & c_{HH2LH2}(k_x,k_y,\zeta) & 0 & E_{HH2}(k_x,k_y) - E
\end{bmatrix}
$$

24

Δ(2)

L

Δ(4)

Δ(6)

764
meV

364 meV

Δ(4)

relaxed
Si$_{0.5}$Ge$_{0.5}$
buffer
layer

Δ(2)

280 meV

hh

502 meV
= V$_{lh}$

lh
so

836 meV
= V$_{hh}$

lh, hh

496 meV

lh
hh

Si   Ge   Si   Ge

applied bias voltage

contact

laser emission

silicon substrate

p Si$_{0.25}$Ge$_{0.75}$ spacer

p^+ Si$_{0.45}$Ge$_{0.55}$ emitter

Ge-Si superlattice

10 periods, 21 ML x 7 ML

p Si$_{0.06}$Ge$_{0.94}$ collector

relaxed p Si$_{0.25}$Ge$_{0.75}$

p^+ Si

1.11 Appendix A: Quantum Parallel Laser : A Unipolar Superlattice Interminiband Laser

Quantum Parallel Laser: A Unipolar Superlattice Interminiband Laser

L. Friedman. R. A. Soref. *Senior Member, IEEE,* and G. Sun

Abstract—Designs are given for parallel (rather than cascade) intersubband lasing in superlattice structures of group IV and III–V materials. Structures with population inversion due to coupled wells have minibandwidths too narrow for coherent transport and the incoherent interperiod rates are too small for population of a significant number of periods. A single-well period with local population inversion gives operation in the coherent regime. An example is given for the III–V materials. Both SiGe–Si and Si–ZnS are discussed for intersubband lasing at 1–20 μm.

I. Introduction

THE quantum cascade laser [1] (QCL) has operated at middle and far-infrared wavelengths. For fiber-optic communications, it would be advantageous to operate this laser at 1–3-μm wavelengths. However, in the near infrared. the QCL suffers from two problems: the bias voltage V_a is high ($V_a \sim MV_p$, where M is the number of periods and V_p is the voltage dropped in one period) and the electric field F approaches or exceeds the breakdown strength ($F \sim V_p/P$. where P is the period width). To deal with these problems. we have proposed and analyzed a new, noncascaded intersubband laser structure, the quantum parallel laser (QPL) whose voltages and fields are low at 1–3-μm emission wavelengths. Room-temperature operation is expected for a $\lambda \sim 1$ μm QPL. and the QPL superlattice structure is simpler in many respects than the QCL structure. For the quantum-well material, we have focused upon silicon because a silicon-based QPL offers hope of low-cost integration with silicon electronic circuits.

II. Laser Structure

The QPL is a unipolar superlattice laser in which each active period lases in parallel with its neighbor, unlike the QCL wherein a single charge carrier traverses M periods, producing lasing in series. It is however necessary to insure that population inversion is achieved in each period. Specifically, in our superlattices (SL), we initially consider three coupled wells for each period, and three bound minibands designed to achieve population inversion between minibands 3 and 2 that are typically heavy-hole valence minibands.
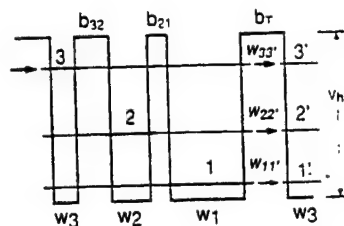
Fig. 1. This three-coupled-quantum-well period of the SL laser is coupled to the next period by resonant tunneling. For $Si_{0.75}Ge_{0.25}$ wells and Si barriers, $w_3 = 10$ Å. $b_{32} = 40$ Å. $w_2 = $ Å 25. $b_{21} = 10$ Å, and $w_1 = 30$ Å. The effective masses are $m_{HH}(Si_{0.75}Ge_{0.25}) = 0.264$ m_0, $m_{HH}(Si) = 0.291$ m_0, where m_0 is the free electron mass.

As shown in Fig. 1. each period includes three QW's and three barriers. with well widths w_3, w_2, w_1 increasing from narrow to wide. giving rise to subband levels $E_3 > E_2 > E_1$. The subscript 3 in w_3 (for example) means that the level-3 wavefunction is localized mainly in that well. Barrier b_{32} is wider than b_{21} reducing the wavefunction overlap between 3 and 2 more than that between 2 and 1. so that the 3–2 transition rate is slower than the 2–1 rate. insuring population inversion. A tunnel barrier b_T is placed between one period and the next period. The complete superlattice interminiband laser is illustrated in Fig. 2(a). where we have shown a p-doped. wider-band-gap emitter for selective injection of holes into the top miniband 3. plus a p-doped collector layer at the far end of the intrinsic (undoped) SL that gathers the charge carriers transmitted from all three levels. A flat-band condition exists across the SL because the applied voltage cancels the built-in voltage due to the work function difference between the injector and collector contacts.

III. Analysis and Calculations

We have performed a rate-equation analysis of Figs. 1 and 2(a). The results are summarized here (the details will be published elsewhere). Here. W_{32} is the phonon scattering rate from level 3 to level 2. while W_{31} and W_{21} are the 3-to-1 and 2-to-1 rates. Also. $W_{33'}$ is the carrier tunneling rate between level 3 of one period and level 3' of the next period ($W_{22'}$ and $W_{11'}$ represent 2-to-2' and 1-to-1' tunneling). In a given period. a fraction $f_{33'}$ of the level-3 hole current is transferred to level 3' of the next period (those fractions are $f_{22'}$ and $f_{11'}$ for levels 2 and 1. respectively). Further, $f_{33'} = W_{33'}/(W_{33'} + W_{32} - W_{31})$, while $f_{22'} = W_{22'}/(W_{22'} + W_{21})$.
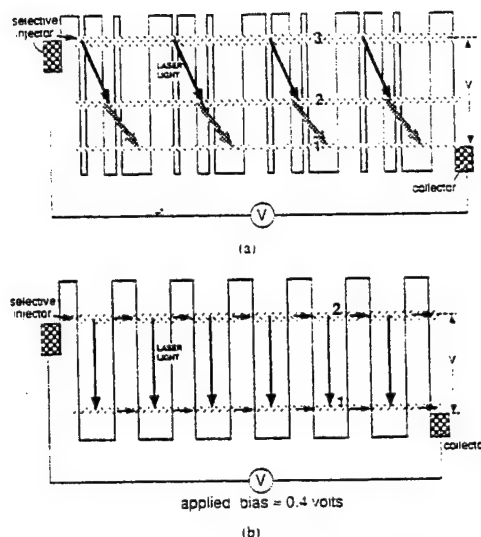
Fig. 2. (a) Band-diagram of the ~ one-volt-biased p⁻-i-p (or n⁻-i-n) unipolar superlattice interminiband QPL showing emitter, collector, 3–2 lasing, and rapid depopulation of 2 by strong 2–1 phonon scattering ($b_{21} < b_{12}$). (b) Band-diagram of single well/barrier superlattice.

The above rates apply to two limiting cases: 1) coherent miniband transport, and 2) incoherent phonon-assisted tunneling. The literature contains several examples of coherent miniband transport [1]–[4] for strongly coupled SL's, a further example being the graded SL coupling regions of the QCL [1]. Because of the long intersubband lifetimes noted below (10–30 ps), the thermal broadening of the levels is smaller than their minibandwidths. However, fluctuations in layer widths and surface roughness will reduce the coherence length, so that case 2) above is the more likely one, especially since the calculated minibandwidths for our proposed SiGe–Si structure are small (<5 meV). Both cases will be discussed below.

We find that population inversion $N_{3i} - N_{2i} > 0$ will occur at each period i (where $i = 1, 2, \cdots, M$), provided that two conditions are met: $W_{21} + W_{22'} > W_{32}$ (level 2 is depleted at a rate faster than it is populated from level 3), and $f_{22'} \ll f_{33'}$ (tunneling 2–2' is much less probable than tunneling 3–3'). When the M identical periods are joined together in a SL, levels 1, 2, 3 become minibands 1, 2, 3. Then the tunnel rates $W_{kk'}$ in the coherent regime [case 1] are obtained as $W_{kk'} = 2B_k/\hbar$, where $\hbar$ is Planck's constant and B_k is the width in eV of miniband k, where $k = 1, 2, 3$. In turn, B_k is dependent upon the tunnel barrier width b_T. For case (2), the $W_{kk'}$ are the rates for acoustical and optical phonon assisted transitions, proportional to the wavefunction overlap between adjacent periods. Because $W_{11'}, W_{22'} < W_{33'}$, space charge buildup will occur toward the collector, giving a redistribution of the voltage and, if sufficiently large, make case 2) the transport mechanism, even for an ideal structure. The laser gain at stage i is proportional to $(N_{3i} - N_{2i})$. It is important to note that the gain is spatially nonuniform in the Fig. 2 QPL

because the inversion decreases progressively from stage to stage and because of the space charge.

Our long-term goal is interminiband lasing at $\lambda = 1.55$ μm, corresponding to an 800-meV intersubband energy difference. Such an energy difference in Si QW's requires large valence-band offsets between Si and the barrier material ($V_{hh} \sim 1.5$ eV in Fig. 1): for example, offsets provided by cubic ZnS barriers [5]. However, the relevant carrier-phonon scattering rates in the Si–ZnS heterosystem, a mixed polar/nonpolar system are not known; these are under current investigation. Therefore, to illustrate the operation of the QPL, we consider instead the $Si_{0.75}Ge_{0.25}$–Si SL of [6]. We have used the procedures of [6] to calculate the rates W_{32}, W_{31} and W_{21}. Cryogenic-temperature operation of this SiGe–Si QPL is assumed to avoid absorptive transitions and thermal population of minibands 2 and 3. The choice of b_T will determine how rapidly the gain falls off from stage to stage, via the tunneling rate $W_{33'}$.

For the SiGe well widths, Si barrier widths, and effective masses given in the Fig. 1 caption, we find that the minima of the heavy-hole minibands HH1, HH2, and HH3 are at 52.4, 83.1, and 151.9 meV. Also, we calculate $W_{32} = 0.015$ ps^{-1}, $W_{31} = 0.010$ ps^{-1}, and $W_{21} = 0.100$ ps^{-1}. These correspond to a narrow tunnel barrier $b_T = 20$ Å selected to achieve strong tunneling. For case 1), we calculate that $W_{11'}$, $W_{22'}$, and $W_{33'}$ are 0.037, 0.166, and 1.140 ps^{-1}, respectively, and that $W_{11'}$, $W_{22'}$, and $W_{33'}$ decrease exponentially with b_T. We also find that $f_{22'} = 0.62$ and $f_{33'} = 0.97$. As desired, $W_{21} + W_{22'} \gg W_{32}$ and $f_{22'} < f_{33'}$: so these parameters satisfy the QPL population-inversion conditions. The ratio of laser gain in stage-M of the SL to the gain in stage-1 is $(f_{33'})^M$.

For case 2), the interperiod rates $W_{kk'}$ would have to be comparable to the intraperiod rates W_{32}, W_{31}, W_{21} in order to populate a significant number of periods. The calculation of the interperiod optical-phonon-assisted transition rates follows the procedure of Palmier et al. [7]. Even for a very narrow barrier between adjacent periods (5 Å), we calculate $W_{33'}/W_{32} = 0.15$, $W_{22'}/W_{33'} = 0.03$, and $W_{11'}/W_{33'} = 0.002$, too small for proper operation. The reason is that the barriers within each period required for population inversion also decrease the wavefunction overlap between adjacent periods. The same narrow minibandwidths (1–3 meV) are found for an analogous GaAs–AlGaAs structure [8] for the same reason. Clearly we want a more tightly coupled superlattice exhibiting larger minibandwidths. One very favorable case is a superlattice consisting of a single quantum well and barrier which exhibits intersubband lasing without global population inversion but due to local-in-k-space inversion [9], shown in Fig. 2(b). For a superlattice of 48 Å $Ga_{0.47}In_{0.53}As$ wells and 40 Å $Al_{0.48}In_{0.52}As$ barriers with two minibands, the upper and lower minibandwidths are 44 and 10 meV, respectively, sufficient for coherent transport. The optical phonon-limited lifetime of the upper state is $\tau_{21} = 1.4$ ps [9]. We calculate $f_{22'} = 0.984$ and $(f_{22'})^M = 0.09$ for $M = 150$, comparable to the total number of layers of the QCL [1], [9]. However, due to space charge buildup in the lower miniband, a smaller number of periods may be required in order to maintain the coherent transport. We plan to investigate the feasibility of local-in-k space population inversion in Si quantum wells.

Returning to the Si–ZnS near-infrared QPL, the intersubband energy separations will be many times kT at room temperature, so that absorptive transitions and thermal population of minibands 2 and 3 will be minimal at 300 K. Due to the higher barriers and stronger confinement, the widths of the active regions and tunnel barriers will be typically 10–20 Å, smaller than those in SiGe–Si.

Finally, we compare the quantum efficiency of the QPL with that of the QCL. The internal power efficiency η is defined as the optical power output of the laser per unit of electrical input power. We note that the laser voltage is $(E_3 - E_1)/e$ for the QPL (about one volt) compared to $M(E_3 - E_1)/e$ in the QCL. If we let $h\nu$ denote the laser photon energy, let r ($\ll 1$) denote the probability that a carrier in level 3 makes a radiative rather than nonradiative transition to level 2, and let $f_{33'}$ denote as before the probability that a carrier in three tunnels to level $3'$ of the next period rather than making a nonradiative or radiative transition to level 2 or level 1 of the same period, then it can be shown that $\eta(\text{QPL}) = rh\nu(1 - (f_{33'})^M)/(E_3 - E_1)$ while $\eta(\text{QCL}) = rh\nu/(E_3 - E_1)$. So the efficiency ratio is $1 - (f_{33'})^M$; thus, if we arrange to make $f_{33'})^M$ very small, approaching zero, then the QPL and QCL efficiencies are comparable.

IV. CONCLUSION

Numerical simulations have been performed on quantum-parallel lasing in $Si_{1-x}Ge_x/Si$ at cryogenic temperatures, and estimates given for the case of coherent transport. However, the minibandwiths are smaller than the linewidths, so interperiod transport is by phonon-assisted tunneling. However, the calculated interperiod rates are too small. In general we believe that any period consisting of coupled wells is not satisfactory. However, a superlattice of 48 Å $Ga_{0.47}In_{0.53}As$ wells and 40 Å $Al_{0.48}In_{0.52}As$ barriers exhibiting lasing due to local-in-k-space population inversion [9] operates in the coherent regime. Other structures with larger minibandwidths require additional investigation. The general importance of the QPL is that it is a structurally simple, unipolar, low-voltage intersubband laser, tunable by design over a wide wavelength range.

REFERENCES

[1] J. Faist, F. Capasso, C. Sirtori, D. L. Sivco, A. L. Hutchinson, and A. Y. Cho, "CW operation of a vertical transition quantum cascade laser above $T = 80$ K," *Appl. Phys. Lett.*, vol. 67, pp. 3057–3059, 1995.

[2] P.-F. Yuh and K. L. Wang, "Novel infrared band-aligned superlattice laser," *Appl. Phys. Lett.*, vol. 51, pp. 1404–1406, 1987.

[3] H. J. Hutchison, A. W. Higgs, D. C. Herbert, and G. W. Smith, "Observation of miniband transport in GaAs/Al$_{0.33}$Ga$_{0.67}$As superlattices," *J. Appl. Phys.*, vol. 75, pp. 320–324, 1994.

[4] A. Sibille, J. F. Palmier, H. Wang, and R. Planel, "Negative differential conductance frequency resonances in X valley superlattice minibands," *Appl. Phy. Lett.*, vol. 65, pp. 2179–2181, 1994.

[5] L. T. Romano, R. D. Brigans, X. Zhou, and W. P. Kirk, "Interface structure of ZnS/Si(001) and comparison with ZnSe/Si(001) and GaAs/Si(001)," *Phys. Rev. B*, vol. 52, p. 11201, 1995.

[6] G. Sun, L. Friedman, and R. A. Soref, "Intersubband lasing lifetimes of SiGe/Si and GaAs/AlGaAs multiple quantum well structures," *Appl. Phys. Lett.*, vol. 66, pp. 3425–3427, 1995.

[7] D. Calecki, J. F. Palmier, and A. Chomette, *J. Phys. C*, vol. 17, p. 5017, 1984.

[8] G. Sun and J. Khurgin, "Optically pumped four-level infrared laser based on intersubband transitions in multiple quantum wells: Feasibility study," *IEEE J. Quantum Electron.*, vol. 29, p. 1104–1109, Apr. 1993.

[9] J. Faist, F. Cappaso, C. Sironi, D. L. Sivco, A. L. Hutchinson, M. S. Hybertsen, and A. Y. Cho, "Quantum cascade lasers without population inversion," *Phys. Rev. Lett.*, vol. 76, no. 3, p. 411–414, 1996.

1.12 Appendix B: Silicon- Based Interminiband Infrared Laser,

Silicon-based interminiband infrared laser

Lionel Friedman[a] and Richard A. Soref
Sensors Directorate. Air Force Research Laboratory. Hanscom Air Force Base. Massachusetts 01731-2909

Gregory Sun
Department of Physics. University of Massachusetts at Boston. Boston. Massachusetts 02125

Simulations of a room-temperature p-i-p coherently strained $Si_{0.5}Ge_{0.5}/Si$ superlattice quantum-parallel laser diode have been made. Calculations have been made of the local-in-k-space population inversion between the nonparabolic heavy-hole valence minibands. HH2 and HH1. Lasing is at 5.4 μm and the optical dipole matrix element is 3.7 A. Analysis of radiative-and-phonon scattering between the "mixed" bands indicates a lifetime difference between the upper and lower states of 2.4 ps. At an injected current density of 5000 A/cm², a laser gain of 134 cm⁻¹ is calculated. © 1998 American Institute of Physics. [S0021-8979(98)05507-8]

I. INTRODUCTION

We recently described the design of a new superlattice interminiband laser called the quantum-parallel laser (QPL).[1] This low-voltage laser operates under flatband conditions. and is much simpler in structure than the well-known quantum-cascade laser (QCL).[2] In addition. the QPL is capable of operating at near-infrared communications wavelengths. as well as middle-infrared wavelengths. unlike the QCL in which the electric field exceeds the dielectric breakdown strength[3] when the laser photon energy approaches 0.8 eV.

The purpose of this article is to show. by calculation. the physical principles of operation of such a silicon-based QPL. The silicon QPL would be capable of integration with advanced silicon microelectronics. We shall consider a $Ge_{0.5}Si_{0.5}/Si$ QPL comprised of identical. square quantum wells. Though there are four minibands, only two are active. The lasing wavelength is at 5.4 μm. Transitions are in the valence band and population inversion is local in k_x space[4] (k_x is the inplane momentum) due to the strong valence band nonparabolicity. Lifetimes are further enhanced by phonon confinement.[5] A gain of $G_L = 134$ cm⁻¹ is calculated for a current density of $J = 5000$ A/cm².

II. LASER MODEL SYSTEM

The band-edge diagram of our proposed. electrically pumped. unipolar. Si-based QPL is shown in Fig. 1. We consider a Ge_xSi_{1-x}/Si superlattice (SL) with $x = 0.5$ to obtain a large valence band offset needed to increase the lasing energy. As shown in Fig. 1. we have chosen the Ge_xSi_{1-x} well width $W = 2.5$ nm. the Si barrier width $B = 1.5$ nm. and the period is $P = W - B = 4.0$ nm. The SL is grown on a (100) silicon substrate. For $x = 0.5$. the critical thickness of the compressively strained Ge_xSi_{1-x} layers is 4 nm for stable strain and 10 nm for metastable stain. For the SL stack as a whole, with a mean Ge concentration of $x = 0.313$. the critical

thickness is 40 nm for metastable strain. Hence with a period of 4 nm. up to ten periods may be grown pseudomorphically: four periods will be used in our calcuations. Hole injection is from a larger band-gap p-SiGe emitter through a thin Si injection barrier: the larger band gap of the emitter insures selective injection into the bottom of the upper HH2 miniband as discussed below. Holes are coherently transported through the SL on the upper miniband. Holes that fall into the lower miniband HH1 are collected via tunneling through a thin Si barrier. thereby depleting that miniband.

As shown in Fig. 1. the heavy-hole (HH) valence band offset at $k = 0$ is $V_{HH} = 450$ meV and the light-hole (LH) offset is $V_{LH} = 371$ meV. For the well. the effective masses are $m_{HH} = 0.24m_0$ and $m_{LH} = 0.178m_0$. while for the barrier $m_{HH} = 0.291m_0$ and $m_{LH} = 0.200m_0$.[6] Four minibands are formed: The HH1 miniband with a 21 meV bandwidth extends from 96 to 117 meV at the miniband zone boundary $k_z = \pi/P$. where k_z is the superlattice wave vector and z is the growth direction. The LH1 miniband extends from 176 meV at $k_z = 0$ to 228 meV at $k_z = \pi/P$. The HH2 miniband is inverted in the $E - k_z$ plane. with a minimum at 347 meV at $k_z = \pi/P$, is 115 meV wide. and extends into the continuum. The LH2 miniband is highest in energy and plays no role. We will comment on the role of the split-off band later in the article. All energies are referenced to the well's HH band edge.

III. INTERSUBBAND LASER OPERATION

Figure 2 shows a schematic of hole energy E as a function of k_x and k_z where x is a direction in the layer plane. Holes are selectively injected near the very bottom of the HH2 miniband at $k_z = \pi/P$. Thus the initial state for the radiative and nonradiative phonon intersubband transitions is at the energy minimum of HH2 at $k_z = \pi/P$ and $k_x = 0$.

For the radiative processes. photon emission is vertical at $k_x = 0$ as shown by the wavy line. Radiation is from $E_{HH2}(k_z = \pi/P)$ to $E_{HH1}(k_z = \pi/P)$, with $[E_{HH2}(k_z = \pi/P) - E_{HH1}(k_z = \pi/P)] = 230.5$ meV. corresponding to a wavelength of $\lambda = 5.36$ μm. and is p polarized (along the z axis).

[a]Electronic mail: friedman@maxwell.rl.plh.af.mil

J. Appl. Phys., Vol. 83, No. 7, 1 April 1998

Friedman, Soref, and Sun   3481

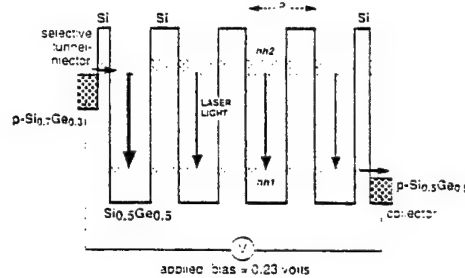

FIG. 1. The quantum-parallel laser: $p - i - p$ diode showing lasing between two valence minibands of $Si_{0.5}Ge_{0.5}/Si$ superlattice. The heavy line is the band edge for heavy holes (HH).

FIG. 3. Waveguided unipolar SiGe/Si superlattice interminiband laser in silicon-on-insulator. Fabry–Perot resonator is shown.

This is the lasing transition. Weaker photon emission from $E_{HH2}(k_z = \pi/P)$ to $E_{LH1}(k_z = \pi/P)$ is s polarized (along the x axis) and has a finite dipole matrix element due only to the admixture of conduction band wave functions into LH1. The first transition is easily distinguished from the second by its polarization and propagation direction and, with suitable optical feedback (resonator geometry), is made the lasing transition. A ridge-waveguide laser cavity with a TM fundamental mode is most suitable for the z-polarized radiation. A bulk silicon substrate could be employed for the resonator because the spatially averaged index of refraction for the superlattice is larger than that of silicon ($\Delta n \sim 0.2$). However, a silicon-on-insulator (SOI) platform is preferred because the buried SiO_2 layer gives a much larger index difference ($\Delta n \sim 2$) between the superlattice and the substrate. The SOI provides high Q, good mode confinement, and a high mode overlap factor. Figure 3 illustrates the proposed rib laser configuration with vertical end facets in a Fabry-Perot cavity.

Consider next the nonradiative processes: At the bottom of the HH2 miniband at $k_z = \pi/P$, the miniband group velocity is very small. At room temperature, the probability of optical phonon emission is proportional to $[1 - n(\omega_{opt})]$, where

$$n(\omega_{opt}) = [\exp(\hbar\omega_{opt}/kT) - 1]^{-1}. \qquad (1)$$

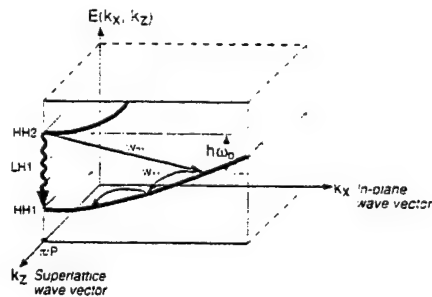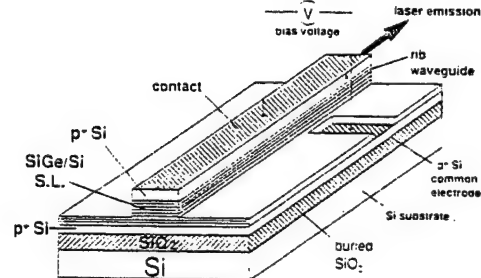FIG. 2. Dispersion of lowest-three valence minibands of $Si_{0.5}Ge_{0.5}/Si$ superlattice as a function of k_x and k_z. W_{21} is the intersuband transition rate and W_{11} is the intrasuband rate.

The emission probability is a factor of 7.25 larger than that of phonon absorption, which is proportional to $n(\omega_{opt})$, and this factor is still larger at lower temperatures. For the $Ge_{0.5}Si_{0.5}$ alloy, the averaged optical phonon energy is taken as 51 meV. Holes absorbing a phonon are scattered to the center of the HH2 miniband where they rapidly transit the superlattice and are not available for lasing. However, at 300 K, the probability of thermal promotion of holes to the center of the upper miniband via optical phonon absorption is only 0.12. By careful selective injection into the bottom of the upper miniband state with small group velocity, hole leakage current to the p-type Si collector due to tunneling from this excited state is avoided, to within the above phonon branching ratio. Another reason for believing that 300 K laser operation is feasible is that the thermal excitation of holes from HH1 to HH2 is negligible at 300 K.

Turning now to the nonradiative HH2-HH1 transition in Fig. 2, emission of an optical phonon from HH2 occurs to superlattice states of finite in-plane momentum, k_x, from which the holes cascade down via intrasubband phonon emission. More exactly, as shown, the final states are on a curve which is the intersection of the energy surface $E_{HH1}(k_x, k_z) = E_{HH1}(k_z) - E_{HH1}(k_x)$ and the horizontal plane $E_{HH2}(k_x = 0, k_z = \pi/P) - \hbar\omega_{opt}$. We will assume that the holes relaxing into HH1 are distributed over the lower miniband and transit the SL at the mean miniband velocity in calculating the tunnel time below. However, in the calculation of optical phonon scattering rates, we shall consider only the in-plane transition at $k_z = \pi/P$, in the interest of calculational simplicity.

Due to the interactions between the HH and LH states, the in-plane valence band dispersion is highly nonparabolic. As shown in Fig. 4, $E_{HH1}(k_x)$ is forced to lower hole energies, $E_{HH2}(k_x)$ is forced to higher hole energies, and $E_{LH1}(k_x)$ becomes electron-like at $k_x = 0$. Thus the energy difference $[E_{HH1}(k_x) - E_{HH2}(k_x)]$ increases with increasing k_x and the photon emitted at $k_x = 0$ cannot be reabsorbed as the hole cascades down the $E_{HH1}(k_x)$ dispersion curve, until it reaches the minimum. More exactly, reabsorption will occur when the absorbed photon is within the linewidth of the upper level. We therefore have a local in k-space inversion as had been described for the InGaAs/InAlAs system by Faist et al.[4] except that here the intersubband energy differ-
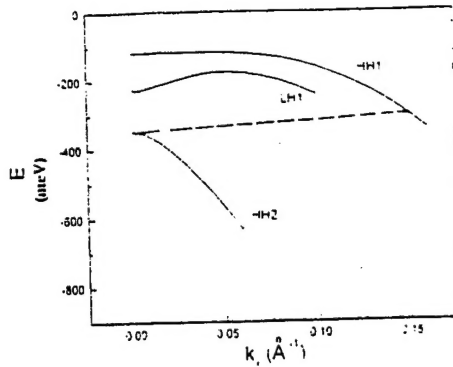
FIG. 4. In-plane dispersion $E = E(k_x)$ of HH1, HH2, and LH1 bands at minizone boundary $k_z = \pi/P$ of $Si_{0.5}Ge_{0.5}/Si$ superlattice, solid lines. Dashed lines are in the absence of interaction ($b = c = 0$). The long dashed straight line shows the intersubband optical phonon emission. Decreasing electron energy (increasing hole energy) is in the downward direction.

ence increases rather than decreases with k_x: explicit calculation shows that at $k_x = 0.02$ A^{-1}, $[E_{HH1}(k_x) - E_{HH2}(k_x)]$ has increased by 50 meV as compared to its value at $k_z = 0$. At each step of the cascade, the hole can either make an downward intrasubband transition by optical phonon emission or tunnel to the collector. Thus the tunnel lifetime of the lower level is decreased by the probability that the hole cascades to the minimum without tunneling to the collector. This decreases the effective lifetime of the lower level and so increases the lifetime difference between the upper and lower lasing levels, enhancing the population inversion.

This lifetime difference is further enhanced by phonon confinement: namely, earlier calculations[5] of phonons confined to a $Ge_{0.5}Si_{0.5}$ layer with Si barriers gives a factor of 3 enhancement of the intersubband lifetimes due to confinement [cf. Fig. 5(a) of Ref. 5], while the intrasubband lifetime is reduced approximately by a factor of 2 [cf. Fig. 4(a) of Ref. 5].

It may appear that the existence of two nonradiative decay paths for the hole in the initial HH2 state, namely to HH1 and to LH1, would result in too small a lifetime for the initial state. However, with increasing in-plane momentum k_x, the HH1 envelope function acquires an admixture of light-hole wave function, while the LH1 acquires heavy-hole character. It is known for bulk materials that the HH to LH transition rate is one to two orders of magnitude smaller than the HH to HH rate[7] due to the smallness of the overlap of the periodic part of the Bloch functions belonging to different energy bands.[3] We assume that same applies to confined valence-band states so that the HH to LH rate may be neglected compared to the HH to HH rate. Thus the net optical phonon emission rate from HH2 to "HH1" is decreased, this being compensated for by an increase in the HH2 to "LH1" rate. Thus the intersubband scattering rate from HH2 is not increased due to the presence of LH1. This is explicitly accounted for in the calculations below.

IV. MODELING OF SiGe IN-PLANE DISPERSION

The SiGe quantum wells' in-plane dispersion diagram is required for the laser gain calculation. To model the in-plane valence band dispersion, we follow the procedure of Bastard.[9] The starting point is the [4×4] Luttinger matrix multiplying the 4-column state vector whose components are the envelope functions at $k_x = 0$ corresponding to the 3/2,3/2), 3/2,−1/2), 3/2,1/2), and 3/2,−3/2) states, respectively, and is given by Eqs. (A1) and (A2) of the Appendix. As shown there in detail, the procedure is to expand the envelope functions at $k_x = 0$ in the bound state envelope functions at $k_x = 0$, cf. Eq. (A3). From these we obtain Eqs. (A4)–(A7).

This procedure leads to a $2(m − n) \times 2(m − n)$ matrix, the diagonalization of which gives the $E(k_x)$ diagram. For the particular superlattice structure described above, there are two bound HH states ($m = 2$) and two bound LH states ($n = 2$), at $k_z = \pi/P$. As explained in the Appendix, the matrix is of dimension $2(m − n) \times 2(m − n)$, leading to the 8×8 shown in Table I. The eigenvalues of this matrix as a function of k_x gives the in-plane dispersion.

V. RESULTS OF IN-PLANE DISPERSION CALCULATION

Because the wells have a center of symmetry, the off-diagonal components of O (e.g., $O_{HH1,LH2}$) and the diagonal components of P (e.g., $P_{HH1,LH1}$) given by Eq. (A9), vanish. For the other components, by numerical integration, we obtain: $O_{HH1,LH1} = 0.9997$, $O_{HH2,LH2} = 0.9932$, $P_{HH1,LH2} = −P_{LH2,HH1} = 0.0798$, $P_{HH2,LH1} = −P_{LH1,HH2} = 0.07820$. Solving for the eigenvalues of the matrix by standard procedures, we obtain the in-plane dispersion curves shown in Fig. 4; here electron energy is negative in the downward direction corresponding to positive hole energy. The dotted curves are the parabolic dispersions in the absence of interaction ($b = c = 0$). It is noted that the lowest eigenvalue $E_{HH1}(k_x)$ is repelled to lower energies, increasing its in-plane effective mass, a general result as pointed out by Bastard.[9] On the other hand, $E_{HH2}(k_x)$ is repelled to higher hole energies so that the difference $[E_{HH1}(k_x) − E_{HH2}(k_x)]$ increases with k_x; this is opposite to the usual conduction band nonparabolicity which gives a larger mass with increasing energy, thereby decreasing the energy difference with k_x. This situation is consider more satisfactory in supressing intersubband absorption at finite k_x. The intermediate $E_{LH1}(k_x)$ dispersion is electron-like at $k_x = 0$.

At $k_z = \pi/P$, the intersubband optical phonon emission from HH2 at $k_x = 0$ goes to HH1 at $k_x = 0.1485$ A^{-1}. This is 180 meV above the HH1 minimum at $k_x = 0$, so three intra-subband optical phonon emissions occur ($\hbar\omega_{opt} = 51$ meV), bringing the hole to within 25 meV from the minimum. Similarly, the intersubband transition from HH2 goes to LH1 at $k_x = 0.115$ A^{-1}.

Finally, we comment on the neglect of the split-off (SO) band in the above analysis. Even at $k = 0$, the SO band will interact with the LH band[10] and perturb the band-edge energies by tens of meV; this is neglected here. The valence band offset of the SO band is shallow, only 110 meV with respect to the SO level of the Si barrier.[6] This together with the small

SO effective mass (0.07 meV at $x = 0.5$) gives a wide SO1 miniband whose energy at $k_z = \pi/P$ is 526 meV above the minimum of HH2 at 347 meV. The SO band will generally repel all the bands to higher (more positive) energies.[11] We are assuming that the altered nonparabolicity allows the local-in-k-space mechanism to be operative. The inclusion of the SO band would require further investigation.

VI. NUMERICAL ESTIMATES OF TRANSITION RATES

Assuming unconfined phonons, the nonpolar optical phonon transition rate from state i to state j is given by[12,13]

$$W_{ij}^{\mp} = (m^* D_0 / 4\pi\rho\hbar^2 \omega_{opt})[n(\omega_{opt}) - 1/2 \mp 1/2]I_{ij}. \quad (2)$$

where[5] $m^* = m_{HH}$. $D_0 = 8.7 \times 10^8$ eV/cm is the optical deformation potential.

$$\rho = 3.83 \text{ gm/cm}^3 \quad (3)$$

is the mass density of the $Ge_{0.5}Si_{0.5}$ alloy. $\hbar\omega_{opt} = 51$ meV is the optical phonon energy of the alloy,[5] $n(\omega_{opt}) = 1/[\exp(\hbar\omega_{opt}) - 1]$ is the phonon population. $I_{ij} = \int dq_z |G_{ij}(q_z)|^2$. and $G_{ij}(q_z) = \langle i|\exp(iq_z z)|j\rangle$ is the hole-phonon overlap factor. By numerical integration, we obtain $I_{HH2-HH1} = 0.115 \text{ A}^{-1}$ (intersubband). $I_{HH1-HH1} = 0.255 \text{ A}^{-1}$ (intrasubband), giving

$$\tau_{inter}^{i} = 1/W_{HH2-HH1} = 0.74 \text{ ps.} \quad (4)$$

$$\tau_{intra} = 1/W_{HH1-HH1} = 0.33 \text{ ps.}$$

Applying the previously mentioned corrections due to phonon confinement.[5]

$$\tau_{inter} = 2.22 \text{ psec.} \quad \tau_{intra} = 0.16 \text{ ps.} \quad (5)$$

Strictly, these correction factors apply to an isolated well[5] but here we assume they apply to a superlattice. To take into account the intersubband transitions to both HH1 and to LH1, we calculate the normalized eigenvectors corresponding to the specific final state energies. As stated above, the initial HH2 state is at $E_{HH2} = -347$ meV. $k_z = \pi/P$, $k_x = 0$. The final HH1 state at $E_{HH1} = -296$ meV, $k_z = \pi/P$, $k_x = 0.1485 \text{ A}^{-1}$. Substituting these values into the eight equations given by Eqs. (A4)–(A7), we find two degenerate eigenvectors corresponding to the Kramers degenerate levels $|3/2,3/2\rangle$ and $|3/2,-3/2\rangle$, namely, $(\alpha_1,\alpha_2,\beta_1,\beta_2,\gamma_1,\gamma_2,\sigma_1,\sigma_2) = (0.537,0,0.731,0,0,-0.287i,0,0.306i)$ and $(0,-0.306i,0,0.287i,0.731,0,0.537,0)$. For the final LH1 state at $k_z = \pi/P$, $k_x = 0.115 \text{ A}^{-1}$, we obtain: $(0.446,0,-0.433,0,0,-0.61i,0,-0.49i)$ and its degenerate counterpart. Subtracting out the probabilities of the light-hole components, the net effect of the wavefunction mixing is to increase τ_{inter} by a factor of approximately $(0.8)^{-1} = 1.25$. Thus, $\tau_{inter} = 2.8$ ps as compared to $\tau_{inter} = 2.22$ ps given in Eq. (5).

VII. TUNNELING RATE TO COLLECTOR

Holes exit the superlattice from the lower miniband through a thin tunnel barrier to the collector. The center of the lower miniband is at an energy of 107 meV, the barrier height is $V = V_{HH} = 450$ meV, $(m_w/m_0) = 0.24$, $(m_b/m_0) = 0.29$, and we take the Si barrier to be five monolayers

wide. $2a = (5 \text{ ML}) = 0.7$ nm. Defining the tunnel amplitude[14] $A(E,a,V)$ as the amplitude of the incident wave transmitted through the barrier, we have

$$A(E,a,V) = \exp[i2k(E)a]/\{\cosh[2\kappa(E,V)a]$$
$$- i[\epsilon(E,V)/2]\sinh[2\kappa(E,V)a]\},$$

where $k(E) = [(E/E_0)(m_w/m_0)]^{1/2}$. $\kappa(E,V) = [(V-E)/E_0] \times (m_b/m_0)]^{1/2}$. and

$$\epsilon(E,V) = [\kappa(E,V)/k(E)](m_w/m_b) - [k(E)/\kappa(E,V)]$$
$$\times (m_b/m_w). \quad (6)$$

The tunnel probability is $T(E,a,V) = |A(E,a,V)|^2$.

We calculate: $T(E,a,V) = 0.291$. This is assumed to be independent of the transverse (in-plane) energy. The mean velocity of the lower miniband is $v = \Delta E^* P/2h = 6.4 \times 10^6$ cm/s. where $\Delta E = 21$ meV is the width of the lower miniband. Assuming the superlattice to consist of four periods, its length is $L = 16$ nm and the time to transit the structure is $t_{tr} = L/v = 0.25$ ps. The tunnel rate is the transit rate multiplied by the tunnel probability $W_{tun} = (1/t_{tr})^* T(E,a,V)$, and the tunnel time is

$$\tau_{tun} = 1/W_{tun} = 0.86 \text{ ps.} \quad (7)$$

As pointed out by the Lucent Technologies work on the local in k-space mechanism,[4] at each stage of the intrasubband cascade, the hole may tunnel to the collector. The probability at each stage that it cascades down rather that tunnels is $W_{intra}/(W_{intra} + W_{tun}) = \tau_{tun}/(\tau_{tun} + \tau_{intra}) = 0.84$. There are three cascades, so the hole can tunnel or undergo intrasubband scattering at four junctures. Thus the probability that the hole reaches the minimum is $[\tau_{tun}/(\tau_{tun} + \tau_{intra})]^4 = 0.5$, and the effective tunnel time is $(\tau_{tun})^{eff} = \tau_{tun}^* [\tau_{tun}/(\tau_{tun} + \tau_{intra})]^3 = 0.43$ ps.

In summary, having applied the correction factors, the lifetimes are

$$\tau_{inter} = 2.8 \text{ ps.} \quad (8)$$

$$(\tau_{tun})^{eff} = 0.43 \text{ ps.}$$

VIII. EMITTER AND COLLECTOR CONTACTS

The collector is (bulk) $Si_{0.5}Ge_{0.5}$ doped p type with boron to 2×10^{19} cm^{-3}. This brings the quasi-Fermi level of the collector 30 meV above the band edge, which is well below the bottom of the lower miniband at 96 meV. We have assumed a 3D density of states effective heavy-hole mass[15] of $m = 1.0m_0$ at 300 K. For the emitter contact, a $Ge_{0.3}Si_{0.7}$ alloy is chosen. Its heavy-hole band edge is 260 meV below that of the silicon substrate and the silicon barriers of the superlattice. When doped to 2×10^{19} cm^{-3} boron, the quasi-Fermi level of the emitter is just at the bottom of the upper miniband, as required. The thickness of the silicon tunnel barrier from the emitter is chosen to be the same as the collector barrier, 5 ML or 7 A.

IX. LASER GAIN

The gain is written[12]

$$G_L = \sigma_{21}(N_2 - N_1)r. \tag{9}$$

where the lasing cross section is $\sigma_{21} = (4\pi\alpha_0/n_0) \times (E_L/\Gamma)|z_{HH2\cdot HH1}|^2$. with $\alpha_0 = 1/137$. the fine structure constant. $n_0 = 3.5$. the refractive index. $E_L = 230.5$ meV. the lasing energy. Γ is the linewidth of $E_{HH2}(k_z)$ at $k_z = \pi/P$. since the initial state is at $k_z = \pi/P$; we choose $\Gamma = 10$ meV. $z_{HH2\cdot HH1}$ is the dipole matrix element for the lasing transition. where $z_{HH2\cdot HH1} = \langle HH2|z|HH1\rangle = \int_0^P \phi_{HH2}(z)^* z \phi_{HH1}(z)dz$.

Here. $|HH1\rangle = \phi_{HH1}(z)$ and $|HH2\rangle = \phi_{HH2}(z)$ are the envelope functions at $k_x = 0$ and $k_z = \pi/P$ and satisfy antiperiodic boundary conditions. $\phi_{HHi}(0) = -\phi_{HHi}(z=P)[i=1,2]$. We obtain $z_{HH2\cdot HH1} = 3.7$ A. The factor $r = 7/8$ in Eq. (9) is the phonon branching ratio described in Sec. II, cf. Eq. (1) et seq.

The population inversion difference is found from a rate equation for the coupled two level system:

$$(N_2 - N_1) = (J/e)\tau_{inter}[1 - (\tau_{tun})^{eff}/\tau_{inter}]. \tag{10}$$

where J is the charge current density and e is the electronic charge. We calculate $(N_2 - N_1) = 7.4 \times 10^{10}$ cm^{-2}. and $G_L = 134$ cm^{-1} for $J = 5000$ A/cm^2. The gain is proportional to the current density. and since the emitter and collector Fermi levels are at the bottom of the upper and lower minibands. respectively. the applied voltage required for the flatband condition is $V_a = 0.23$ V. G_L is inversely proportional to the value taken for Γ.

X. CONCLUSIONS

Simulations of a room-temperature p-i-p coherently strained Si$_{0.5}$Ge$_{0.5}$/Si superlattice quantum-parallel laser diode have been made and a waveguided SOI resonator structure has been proposed. Calculations have been made of the local-in-k-space population inversion between the nonparabolic HH2 and HH1 valence minibands at the 5.4 μm laser wavelength where the dipole matrix element is 3.7 A. Analysis of radiative-and-phonon scattering between the "mixed" bands indicates a laser lifetime difference of 2.4 ps. The non-radiative intersubband optical phonon scattering is slower than the in-plane intrasubband scattering. The intersubband lifetime is enhanced and the intrasubband lifetime decreased by phonon confinement. The effective lifetime of the lower state is further decreased by the probability of

sequential tunneling to the collector. At a current density of 5000 A/cm^2, a laser gain of 134 cm^{-1} is calculated.

APPENDIX: MODELING OF THE IN-PLANE DISPERSION

The SiGe quantum wells' in-plane dispersion diagram is required for the laser gain calculation. To model the in-plane valence band dispersion. we follow the procedure of Bastard.[9] The starting point is the $[4 \times 4]$ Luttinger matrix multiplying the 4-column state vector whose components are the envelope functions at $k_x \neq 0$ corresponding to the $|3/2,3/2\rangle$. $|3/2,-1/2\rangle$. $|3/2,1/2\rangle$. and $|3/2,-3/2\rangle$ states. respectively.

$$H_{\Gamma 8} = \begin{vmatrix} H_{hh} & c & b & 0 \\ c^* & H_{lh} & 0 & -b \\ b^* & 0 & H_{lh} & c \\ 0 & -b^* & c^* & H_{hh} \end{vmatrix}, \tag{A1}$$

where

$$H_{hh} = -E_0[(k_x^2 - k_y^2)(\gamma_1 - \gamma_2) - k_z^2(\gamma_1 - 2\gamma_2)] + \epsilon.$$

$$H_{lh} = -E_0[(k_x^2 - k_y^2)(\gamma_1 - \gamma_2) + k_z^2(\gamma_1 - 2\gamma_2)] - \epsilon. \tag{A2}$$

$$c = c(k_x,k_y) = 3^{1/2}E_0[\gamma_2(k_x^2 - k_y^2) - i2\gamma_3 k_x k_y].$$

$$b = b(k_x,k_y) = 2*3^{1/2}E_0(k_x - ik_y)\gamma_3(-i)d/dz$$

$$= b^-(k_x,k_y)d/dz.$$

where ϵ is the uniaxial strain energy. $E_0 = \hbar^2/2m_0 = 3810$ meV* A^2. and the γ_i ($i=1,2,3$) are the Luttinger parameters. At finite k_x. the envelope functions are expanded in the envelope functions at $k_x = 0$:

$$\Psi = \begin{vmatrix} \Sigma_{i=1,m}\alpha_i\Phi_i^{HH} \\ \Sigma_{i=1,n}\beta_i\Phi_i^{LH} \\ \Sigma_{i=1,n}\gamma_i\Phi_i^{LH} \\ \Sigma_{i=1,m}\sigma_i\Phi_i^{HH} \end{vmatrix}, \tag{A3}$$

where there are m bound HH states and n bound LH states at $k_x = 0$. Thus there are a total of $2(m+n)$ coefficients. Equations (A1) and (A3) are substituted into the eigenvalue equation $H_{\Gamma 8}\Psi = E\Psi$. Considering the first row. multiplying to the left by $(\Phi_i^{HH})^*$ and integrating, we obtain

$$\alpha_i(E_{HHi} - E) - \Sigma_{j=1,n}c_{HHiLHj}\beta_j - \Sigma_{j=1,n}b_{HHiLHj}\gamma_j = 0,$$

$$i = 1,....m \tag{A4}$$

TABLE I. 8×8 matrix determining in-plane dispersion.

$M(k_x,k_y,E) =$							
$E_{HH1} - E$	0	c_{HH1LH1}	0	0	b_{HH1LH2}	0	0
0	$E_{HH2} - E$	0	c_{HH2LH2}	b_{HH2LH1}	0	0	0
c_{LH1HH1}^*	0	$E_{LH1} - E$	0	0	0	0	$-b_{LH1HH2}$
0	c_{LH2HH2}^*	0	$E_{LH2} - E$	0	0	$-b_{LH2HH1}$	0
0	b_{LH1HH2}^*	0	0	$E_{LH1} - E$	0	c_{LH1HH1}	0
b_{LH2HH1}^*	0	0	0	0	$E_{LH2} - E$	0	c_{LH2HH2}
0	0	0	$-b_{HH1LH2}^*$	c_{HH1LH1}^*	0	$E_{HH1} - E$	0
0	0	$-b_{HH2LH1}^*$	0	0	c_{HH2LH2}^*	0	$E_{HH2} - E$

where $c_{HHiLHj} = \langle \Phi_i^{HH} | c | \Phi_j^{LH} \rangle$, $b_{HHiLHj} = \langle \Phi_i^{HH} | b | \Phi_j^{LH} \rangle$.

Following the same procedure for the second, third, and fourth rows, we obtain

$$\Sigma_{j=1,m} c_{LHiHHj}^* \alpha_j - \beta_i (E_{LHi} - E) - \Sigma_{j=1,m} b_{LHiHHj} \sigma_j = 0.$$

$$i = 1,...,n; \tag{A5}$$

$$\Sigma_{j=1,m} b_{LHiHHj} \alpha_j - \gamma_i (E_{LHi} - E) - \Sigma_{j=1,m} c_{LHiHHj} \sigma_j = 0.$$

$$i = 1,...,n; \tag{A6}$$

$$-\Sigma_{j=1,n} b_{LHiHHj}^* \beta_j - \Sigma_{j=1,n} c_{LHiHHj}^* \gamma_j - \sigma_i (E_{HHi} - E) = 0.$$

$$i = 1,...,m; \tag{A7}$$

where the following relations hold:

$$c_{LHiHHj}^* = \langle \Phi_i^{LH} | c^* | \Phi_j^{HH} \rangle = (c_{HHjLHi})^*.$$

$$b_{LHiHHj} = \langle \Phi_i^{LH} | b | \Phi_j^{HH} \rangle,$$

$$b_{HHiLHj}^* = \langle \Phi_i^{HH} | b^* | \Phi_j^{LH} \rangle = (b_{LHjHHi})^*.$$

$$c_{HHiLHj}^* = \langle \Phi_i^{HH} | c^* | \Phi_j^{LH} \rangle = (c_{LHjHHi})^*.$$

This procedure leads to a $2(m-n) \times 2(m-n)$ matrix, the diagonalization of which gives the $E(kx)$ diagram. For the particular superlattice structure described above, there are two bound HH states ($m=2$) and two bound LH states ($n=2$), at $\bar{k}_z = \pi/P$, and so the matrix is of dimension 8×8 and is shown in Table I.

In this matrix, all entries are functions of k_x and k_y, and we have set $k_y = 0$. Explicitly,

$$c_{HHi,LHj} = c(k_x, k_y) O_{HHi,LHj} \quad (i,j = 1,2), \tag{A8}$$

$$b_{HHi,LHj} = b^-(k_x, k_y) P_{HHi,LHj}. \quad (i,j = 1,2),$$

where

$$O_{HH1,LH1} = \int dz \phi_{HH1}(z)^* \phi_{LH1}(z).$$

$$O_{HH2,LH2} = \int dz \phi_{HH2}(z)^* \phi_{LH2}(z), \tag{A9}$$

$$P_{HH1,LH2} = \int dz \phi_{HH1}(z)^* [d/dz \phi_{LH2}(z)],$$

$$P_{HH2,LH1} = \int dz \phi_{HH2}(z)^* [d/dz \phi_{LH1}(z)].$$

[1] L. Friedman, R. A. Soref, and G. Sun, IEEE Photonics Technol. Lett. **9**, 593 (1997).
[2] C. Sirtori, J. Faist, F. Capasso, D. L. Sivco, A. L. Huchinson, S. N. G. Chu, and A. Y. Cho, Appl. Phys. Lett. **68**, 1745 (1996).
[3] G. Sun L. Friedman, and R. A. Soref, Superlattices Microstruct. **22**, 3 (1997).
[4] J. Faist, F. Capasso, C. Sirtori, D. L. Sivco, A. L. Huchinson, M. S. Hybertsen, and A. Y. Cho, Phys. Rev. Lett. **76**, 411 (1996).
[5] G. Sun and L. Friedman, Phys. Rev. B **53**, 3966 (1996).
[6] A. Kahan, M. Chi, and L. Friedman, J. Appl. Phys. **75**, 8012 (1994).
[7] N. Nintunze and M. A. Osman, Semicond. Sci. Technol. **10**, 11 (1995).
[8] J. D. Wiley, Phys. Rev. B **4**, 2485 (1971).
[9] G. Bastard, "Wave Mechanics Applied to Semiconductor Heterostructures," Les Editions de Physique, p. 108 (1990).
[10] G. Sun and L. Friedman, Superlattices Microstruct. **17**, 245 (1995).
[11] C. Yi-Ping Choa and S. L. Chaung, Phys. Rev. B **46**, 4110 (1992).
[12] G. Sun, L. Friedman, and R. A. Soref, Appl. Phys. Lett. **66**, 3425 (1995).
[13] B. K. Ridley, J. Phys. C **15**, 5899 (1982).
[14] E. Merzbacher, Quantum Mechanics (Wiley, New York, 1970), p. 94.
[15] Semiconductors, in Group IV Elements and III-V Compounds, edited by O. Madelung (Springer, Berlin, 1991), p. 14.